Scientia Iranica A (2012) 19 (6), 1391–1410

Sharif University of Technology

Scientia Iranica

Transactions A: Civil Engineering

www.sciencedirect.com

Consolidated undrained behavior of gravelly materials

A. Aghaei Araei [a,*], A. Soroush [b], S. Hashemi Tabatabaei [a], A. Ghalandarzadeh [c]

[a] *Department of Geotechnical Engineering, Road, Housing and Urban Development Research Center (BHRC), Tehran, P.O. Box: 13145-1696, Iran*
[b] *Department of Civil and Environmental Engineering, Amirkabir University of Technology, Tehran, P.O. Box: 01232747, Iran*
[c] *Department of Civil Engineering, University of Tehran, Tehran, P.O. Box: 11365-4563, Iran*

Received 27 August 2011; revised 30 July 2012; accepted 8 September 2012

KEYWORDS

Gravelly materials;
Triaxial testing;
CU;
CD;
Excess pore pressure.

Abstract This paper studies the behavior of a number of gravelly modeled materials by conducting large-scale triaxial testing. Undrained monotonic compression tests were carried out on the high compacted gravelly soil specimens with different fine content and stress levels. It was observed that high compacted gravelly soil specimens show dilative behavior at failure in a wide range of fine content. The effective stress paths of the materials having less than 10% and more than 22% of material finer than 0.2 mm are completely different. Variations of the *CU* material parameters with respect to the confining pressure, fine content, shape, strength and particle size were investigated. The CU material results were compared with those in CD conditions. The value of internal effective friction angle in CD conditions is slightly higher than those of the CU conditions. Moreover, where the volume strain in *CD* conditions is minimum, the excess pore water pressure in *CU* conditions decreases to zero.

1. Introduction

Gravelly materials are used in landfills in civil engineering projects including rockfill dams, quay, and road embankment which make the precise knowledge of the behavior of these materials indispensable. For example, stability analysis as well as back-analysis of stress, deformations and excess pore water pressure in rockfill dams requires determination of shear strength parameters and stress-volume change-excess pore water pressure versus strain of the used gravelly materials. The deformation characteristics of undrained behaviors of clay, silt and sandy soils have been frequently studied in recent years. However, the deformation characteristics of gravelly soils under undrained loading have not been studied in depth because: (a) test results on gravelly soils are affected by the membrane penetration phenomenon much more than sandy soils; therefore, in conducting tests on these materials this problem should be solved; and (b) it has been assumed that gravelly soils are less susceptible to liquefaction because of their high permeability; however, drainage may be impeded or permeability can be reduced in some cases [1].

The behavior of gravelly materials is affected by the factors including mineralogical composition, initial relative density, particle grading, fragmentation of particles, size and shape of particles, drainage conditions, moisture content during construction and stress level. Fine contents, stress level and drainage conditions are of the most effective factors on the shear strength of these materials. Testing gravelly materials and modeling their behavior are essential prerequisites to realistic analyses and economic designs of rockfill dams.

Rockfill materials contain particles of large sizes and their testing requires equipments of greater specimen dimensions. Therefore, the sizes of particles for testing are reduced usually using modeling techniques [2–5].

All granular aggregates subjected to stresses above the normal geotechnical ranges exhibit considerable particle breakage [6–9]; however, particle breakage of rockfills may even occur at low confining pressures [10,11]. Particle crushing

* Corresponding author. Tel.: +98 21 88255942x260; fax: +98 21 88255942x319.
E-mail addresses: aghaeiaraei@bhrc.ac.ir (A. Aghaei Araei), soroush@aut.ac.ir (A. Soroush), htabatabaei@bhrc.ac.ir (S. Hashemi Tabatabaei), aghaland@ut.ac.ir (A. Ghalandarzadeh).
Peer review under responsibility of Sharif University of Technology.

Production and hosting by Elsevier

1026-3098 © 2012 Sharif University of Technology. Production and hosting by Elsevier B.V. Open access under CC BY-NC-ND license.
doi:10.1016/j.scient.2012.09.011

Notation

The following symbols are used in this paper:

B_g	Marsal's breakage index
c	Cohesion
CD	Consolidated Drained
CU	Consolidated Undrained
σ_1'	Effective major principal stress
σ_3'	Effective minor principal stress/effective confining pressure
ε_1	Major principal strain
E_m	Young's modulus of the membrane
ε_v	Volumetric strain
ψ	Dilation angle
ϕ	Total stress internal fiction angle
ϕ'	Effective internal friction angle
$\phi_{q_{peak}}$	Internal friction angle at maximum deviator stress
γ_d	Dry density
LA	Los Angeles abrasion
s'	Effective mean principle stress $= (\sigma_1' + \sigma_3')/2$
PI	Plasticity Index
q	Deviator stress
q_{cd}	Deviator stress in CD condition
q_{cu}	Deviator stress in CU condition
q_{max}	Maximum deviator stress
$q_{residual}$	Residual deviator stress
re	Repeated
S_{us}	Undrained residual shearing strength
τ	Shear stress $= (\sigma_1' - \sigma_3')/2$
u	Excess pore water pressure
u_{max}	Maximum excess pore water pressure
W_{opt}	Optimum water content

causes volumetric contraction in drained loading and pore water pressure build up in undrained loading [12].

Generally, alluvial materials show an increase [9,13] and decrease [9] in the angle of shearing resistance as the size of the particles increases depending on the particle strength and the confining pressure, whereas materials produced from rock crushed show a decrease in the angle of shearing resistance as the size of the particles increases [9,13,14].

Undrained shearing behavior of very loose gravelly soils with different gravel contents (30%–90%) was investigated by Rashidian et al. [1] using wet tamping method. Goto et al. [15] pointed out that the negative dilatancy characteristics (negative volumetric strain) of gravelly soils under drained conditions corresponds to the rate of pore pressure build up under undrained conditions.

There is not much research in the literature about the mechanical behavior of highly compacted gravelly materials used in rockfill dams with large scale triaxial tests, especially in *CU* conditions. This paper studies the behavior of a number of gravelly materials by conducting large-scale triaxial testing in *CU* conditions as well as comparison with *CD* results.

2. Materials properties

The materials under study are from the clay core and shell of ten rockfill dams constructed or under construction in Iran.

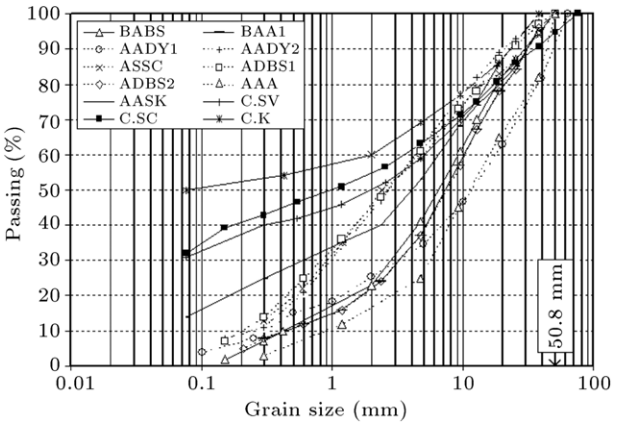

Figure 1: Gradations of the modeled gravelly materials.

Table 1 summarizes the materials characteristics, including rockfill type, mineralogy, size distribution, Los Angeles abrasion (*ASTM C 535*), Point Load Strength index (*ASTM D 5731*), dry density, optimum water content and rate of loading. The maximum dry densities are determined according to *ASTM D1557*. For the purpose of brevity, the names of the materials are introduced with their abbreviations.

3. Experimental program

The gradations of the materials for triaxial testing are derived using the parallel gradation modeling technique [3] with a maximum particle sizes of 50 mm and 39 mm (1/6 and 1/5 diameter of large-scale triaxial cell), as shown in Figure 1. The ranges of confining pressures are chosen according to the stress levels in the dams (50 kPa–1500 kPa). Consolidated Undrained (*CU*) triaxial tests were conducted according to ASTM D 4767 [17]. These tests were conducted on large scale specimens with 200 and 300 mm diameters, and 400 and 600 mm heights, using the large-scale triaxial equipment at the Geotechnical Department of the Road, Housing and Urban Development Research Center (BHRC), Tehran, Iran.

4. Testing procedure

For each of the specimens, the quantity of various sizes of grains required to achieve the gradation of the modeled gravelly material for having the specimen at more than 95% maximum dry density was determined by weight.

A silicone type membrane with a thickness of 2.5 mm complying with ASTM D 4767 [17] was used to encase the specimen and provide reliable protection against leakage. The Young's modulus of the used membrane (E_m) is 750 kPa. The increase of deviator stress for $\varepsilon_1 = 15\%$ (0.15 in decimal form) is less than 4 kPa. We ignored membrane correction effect over the measured deviator stress. The interaction among the specimen, membrane, and confining fluid influences the static and the cyclic behaviors. Changes in pore-water pressure can cause changes in membrane penetration in specimens of cohesion-less soils, *ASTM D 5311* [18]. It was observed that gravelly specimens prepared by wet tamping method had a fairly smooth surface, i.e. less peripheral voids [1]. We eliminated membrane penetration effects by putting the finer soil in the surface of specimens to create a smooth surface.

Table 1: Characteristics of rockfill materials used in large-scale triaxial testing in CU conditions [16].

	Material	Dam	Symbol	Passing 39.2 mm (%)	Passing 25.4 mm (%)	Passing 4.75 mm (%)	Passing 0.2 mm (%) /Passing 0.075 mm (%)	USCS[b] classification	Los Angeles Abrasion[c] (LA) (%)	Point load index[d] (Is)	γ_d (95%) (kN/m^3)	W_{opt} (%)	Rate of loading mm/min
Blasting	Andesibasalt	Sabalan	BABS[a]	95	72	37	4/NIA	GW	28	5.45	21.1	4.5	0.50
	Andesite	Aydoghmosh-G1	BAA1[a]	96	84	37	8/NIA	GW	19	3.95	21.8	6.5	0.50
Alluvium	Andesite-Dacite	Yamchi-G1	AADY1[a]	80	70	35	7/NIA	GW	32	NIA	20.5	9.0	0.50
		Yamchi-G2	AADY2[a]	98	91	62	10/NIA	SM					0.50
	Alluvium-River Bed	Shahr-Chi	ASSC	94	83	59	10/NIA	SM	NIA	NIA	21.9	5.8	0.50
	Deurite-Basite	Sahand-G1	ADBS1[a]	97	91	62	10/NIA	SM	46	NIA	20.5	9.0	0.50
		Sahand-G2	ADBS2[a]	96	84	37	8/NIA	GW					0.50
	Andesite	Aydoghmosh-G2	AAA[a]	82	73	25	1/NIA	GW	19	NIA	22.3	7.4	0.50
	Andese-Basalt	Sattar-Khan	AASK	95	85	53	22/14	GC	NIA	NIA	20.0	9.0	0.50
Core	Highly Weathered Sandstone, PI = 8.6	Vanyar	C.SV	100	92	59	37/31	GC	NIA	NIA	20.8	9.5	0.10
	Alluvium, PI = 13.5	Shahr-Chi	C.SC	91	86	63	41/32	GC	NIA	NIA	20.3	10.1	0.20
	Alluvium, PI = 30.0	Karkheh	C.K	100	90	69	53/50	GC/CH	NIA	NIA	18.3	13.5	0.07

NIA: no information available.
[a] CD tests were also conducted [16].
[b] Unified soil classification system.
[c] ASTM C 535.
[d] ASTM D 5731.

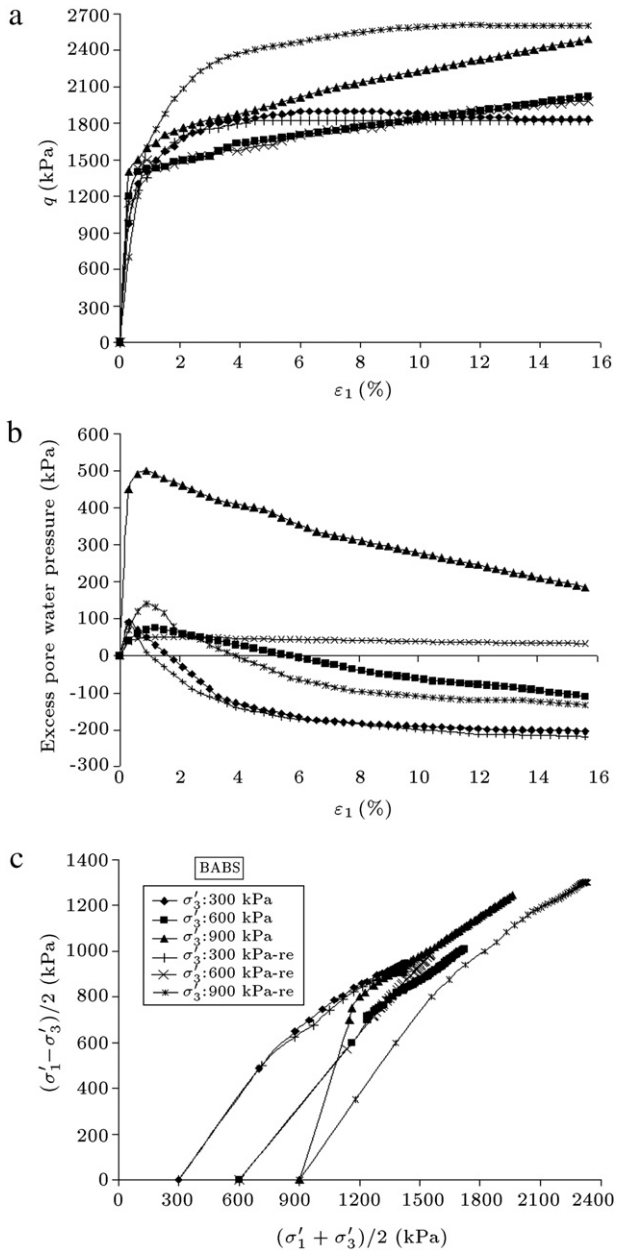

Figure 2: Stress–strain-excess pore water pressure and stress path relationships of BABS.

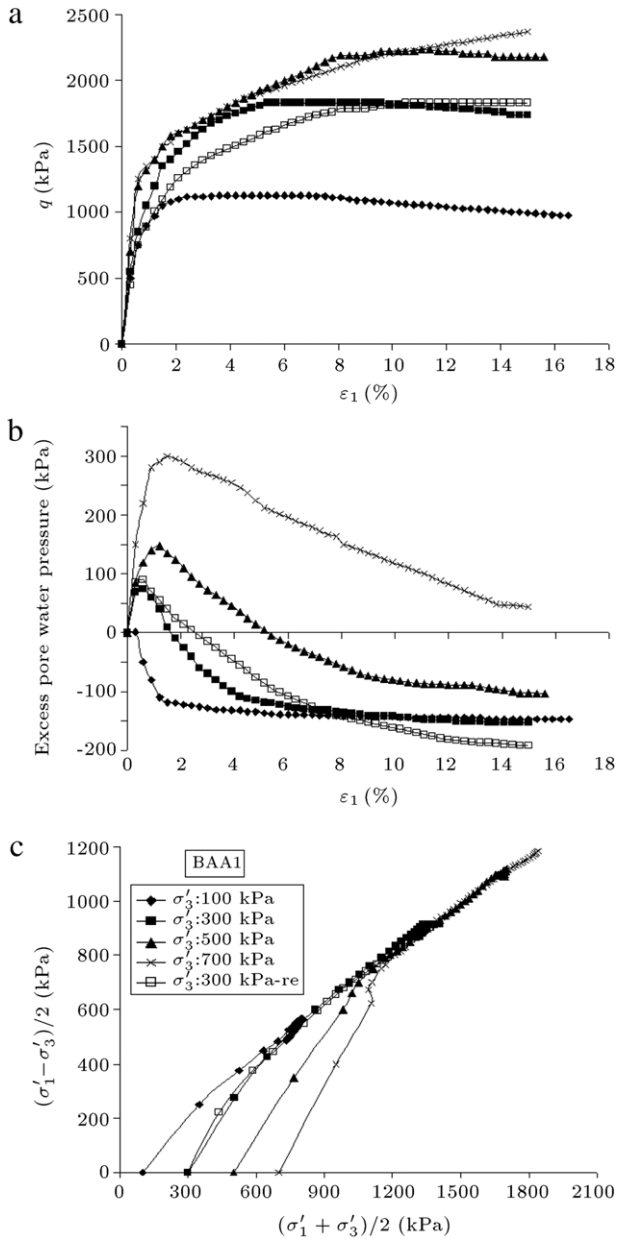

Figure 3: Stress–strain-excess pore water pressure and stress path relationships of BAA1.

The individual fractions were mixed with distilled water to the optimum moisture content. The specimen materials were divided into six equal parts and prepared in six layers inside a split mold. Each of the layers was compacted using a vibrator with frequency of 60 cycles/s. After passing CO_2 and applying vacuum, the specimen was saturated to a *B*-value of 95% by allowing water to enter through the base of the triaxial cell and removing the air bubbles. The specimen was subjected first to the required consolidation pressure and then was sheared to failure in undrained conditions by applying axial loading with a rate of 0.07–0.50 mm/min. A few tests were repeated to verify reproducibility of the results. Axial loading, vertical displacements and excess pore water pressure were monitored and recorded at periodic intervals during the tests.

5. Tests results

5.1. Immediate results

Stress-excess pore water pressure versus axial strain relationships and corresponding effective stress paths of the twelve modeled gravelly materials subjected to *CU* triaxial testing are shown in Figures 2–13. It is observed that, in general, axial strain at failure increases with increasing of confining stress. Generally, increase in confining pressure results in an increased pore pressures in the contractive phase, in the absence of any volume change. Generally, the gravelly materials having less than 10% of the material finer than 0.2 mm showed alternating trends (negative and positive) in their excess pore water pressure behavior, depending on their confining

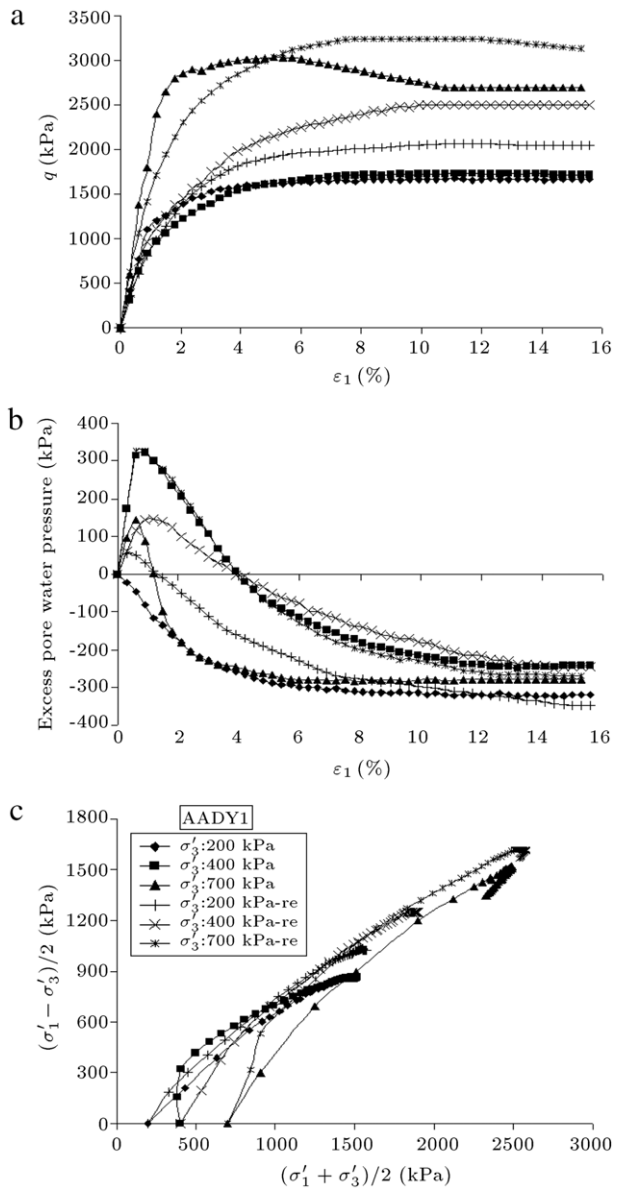

Figure 4: Stress–strain-excess pore water pressure and stress path relationships of AADY1.

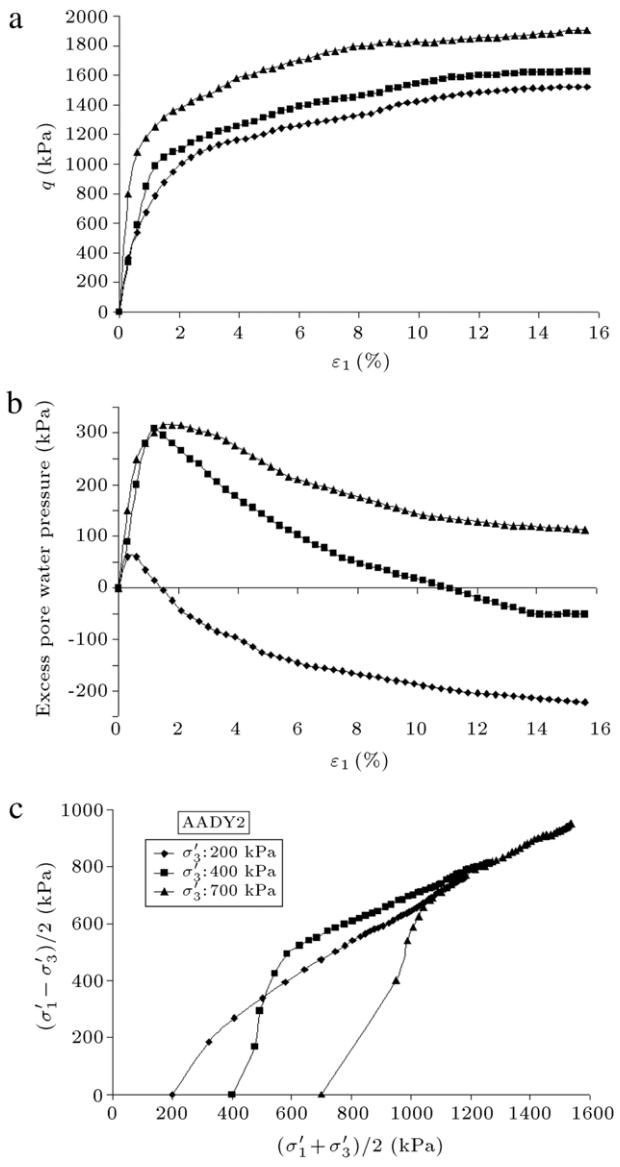

Figure 5: Stress–strain-excess pore water pressure and stress path relationships of AADY2.

pressures (Figs. 2(b) and 9(b)). But, the gravelly materials having more than 22% of material finer than 0.2 mm showed positive excess pore water pressure behavior (Figs. 10(b) and 13(b)).

In the highly compacted specimens a leveling out of the $u : \varepsilon_1$ behavior in the form of negative pore water pressure occurs in some of the specimens at low confining pressures due to the strain localization. At high confining pressures, the highly compacted specimens bulge uniformly in the vicinity of peak stress and develop complex multiple symmetrical radial shear bands at higher axial strain levels [19–22]. It can be seen that the peak in the stress–strain curves appears eminently when the initial confining pressure is small, but the peak tends to dwindle as the initial confining pressure becomes larger.

The $s' - \tau$ stress paths of the gravelly soils having less than 10% of material finer than 0.2 mm are different from materials having more than 22% of material finer than 0.2 mm. So that, in the material having less than 10% of material finer than 0.2 mm, the stress path moves to the right side (dilative behavior) and ends at failure surface (Figs. 2(c)–9(c)), but in the latter, depending on the rate of loading and confining pressure, dilative-contractive or contractive-dilative behaviors may be observed (Figs. 10(c)–13(c)). For example, the stress path of *AASK* at $\sigma'_3 = 200$ kPa is dilative-contractive, while at $\sigma'_3 = 500$ kPa is contractive-dilative.

Depending on the combination of anisotropy, confining pressure and fine contents, gravelly materials may experience a drop in shear strength. The occurrence of such a temporary drop in shear strength at relatively large strains has been named quasi-steady state. It should be noted that the quasi-steady state is affected by the initial confining pressure at consolidation stage; i.e. the bigger the initial confining pressure is, the larger the minimum strength and corresponding effective mean stress will be.

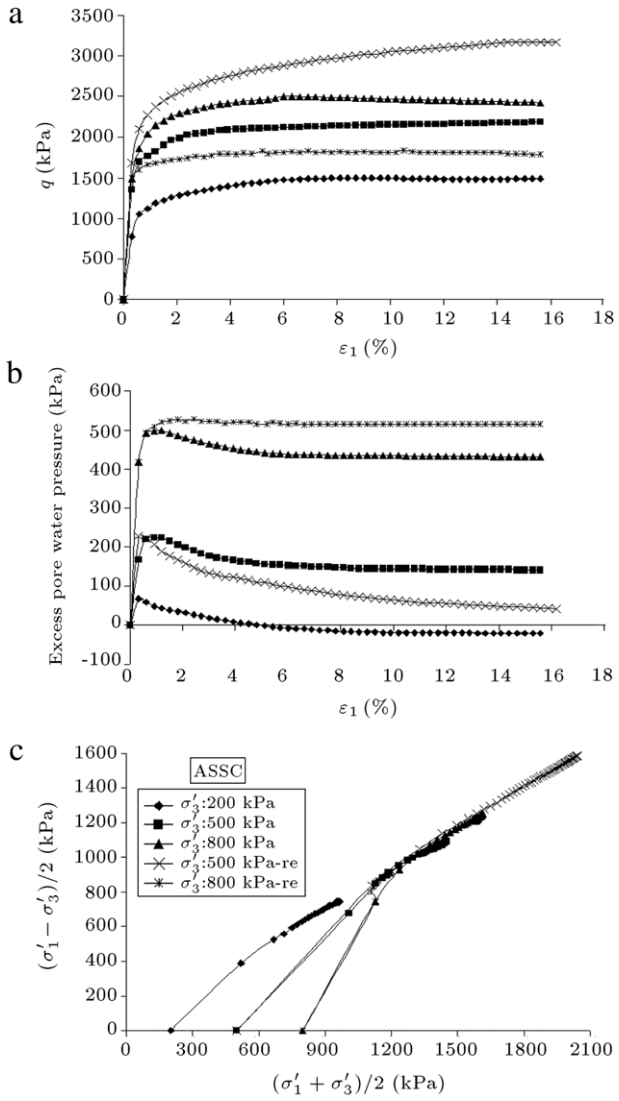

Figure 6: Stress–strain-excess pore water pressure and stress path relationships of ASSC.

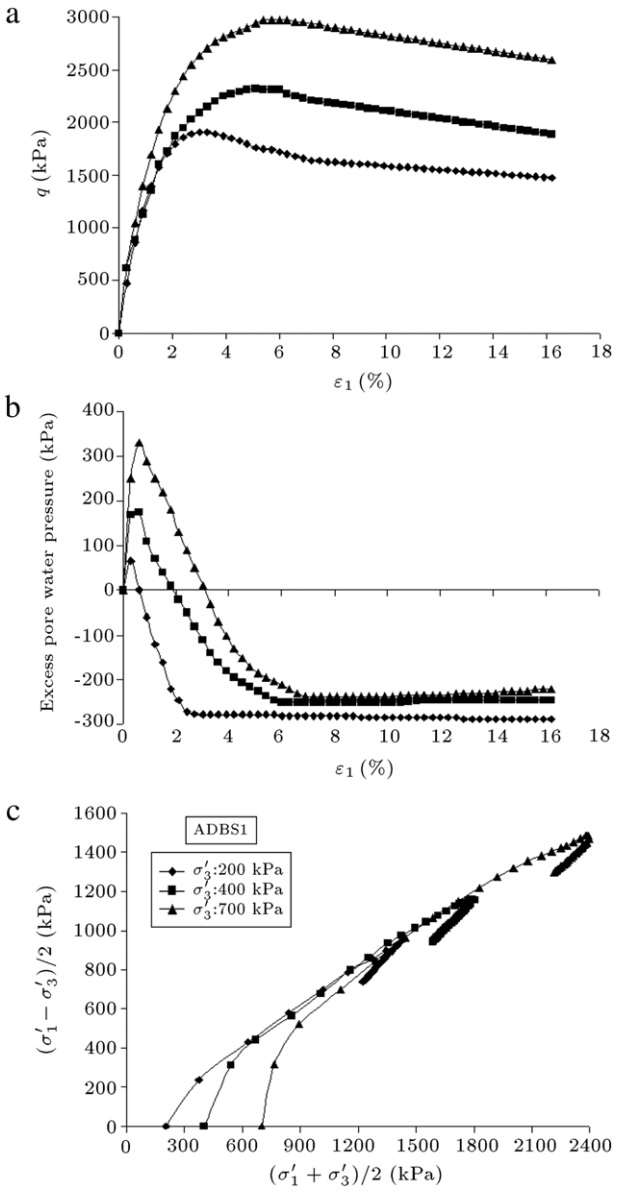

Figure 7: Stress–strain-excess pore water pressure and stress path relationships of ADBS1.

5.2. Compiled results

The compiled results of the tests, such as axial strain, deviator stress, excess pore water pressure, total internal friction angle (ϕ) and effective internal friction angle (ϕ') at axial strains corresponding to maximum excess pore water pressure, maximum deviator stress, and residual deviator stress, are presented in Table 2.

$u_{max} : \sigma'_3$.

Variations of the maximum excess pore water pressure, excess pore water pressure at axial strain corresponding to maximum deviator stress and residual deviator stress versus confining pressure (σ'_3) for the gravelly materials are shown in Figure 14. This figure indicates that almost for all of the gravelly materials, maximum excess pore water pressure is positive and increases as σ'_3 increases. For the gravelly materials having less than 10% of material finer than 0.2 mm, variations of excess pore water pressures (u) at maximum deviator stress and residual deviator stress are negative (i.e., contractive behavior) at low confining pressures and positive at high confining pressures (i.e., dilative behavior). It is interesting to note that the variations of u at residual deviator stress with confining pressures are slightly lower than u at maximum deviator stress, and the difference increases slightly as σ'_3 increases.

The variations of u_{max} and u at maximum deviator stress and residual deviator stress with confining pressures for the gravelly materials having more than 22% of material finer than 0.2 mm are presented in Figure 14. The results indicate that u at maximum deviator stress and residual deviator stress are identical and positive and higher than u_{max} for the gravelly materials having less than 10% of material finer than 0.2 mm as σ'_3 increases.

$q : \sigma'_3$.

Figure 15 shows variations of q/σ'_3 versus σ'_3 at u_{max}, q_{max} and $q_{residual}$ for the gravelly materials having less than 10%

Table 2: Results of triaxial tests on gravelly soils in CU conditions.

Gravelly soils	σ_3' (kPa)	At u_{max}					At q_{max}					At $q_{residual}$			
		ε_1 (%)	q (kPa)	u (kPa)	ϕ (°)	ϕ' (°)	$(\varepsilon_1)q_{max}$ (%)	q_{max} (kPa)	u (kPa)	ϕ (°)	ϕ' (°)	$q_{residual}$ (kPa)	u (kPa)	ϕ (°)	ϕ' (°)
BABS	300	0.3	975	90	38.2	44.3	6.3	1894	−171	49.4	41.9	1830	−204	48.9	40.2
	600	1.2	1430	75	32.9	35.2	15.6	2020	−110	38.9	36.0	–	–	–	–
	900	0.9	1600	500	28.1	41.8	15.6	2488	185	35.5	39.4	–	–	–	–
BABS-re	300	0.3	1000	85	38.7	44.4	10.2	1822	−200	48.8	40.2	–	–	–	–
	600	1.5	1443	51	33.1	34.6	15.6	1975	33	38.5	39.5	–	–	–	–
	900	0.9	1600	140	28.1	30.9	11.7	2608	−119	36.3	34.1	2600	−134	36.2	33.9
BAA1	100	0.3	500	1	45.6	45.8	3.9	1130	−132	58.2	45.1	973	−152	56.0	41.2
	300	0.6	850	75	35.9	40.8	5.4	1830	−120	48.9	43.3	1740	−146	48.0	41.4
	500	1.2	1400	148	35.7	41.7	11.1	2240	−87	43.7	41.0	2180	−104	43.3	40.0
	700	1.5	1500	300	31.1	40.7	15.0	2370	44	39.0	40.1	–	–	–	–
BAA1-re	300	0.9	890	90	36.7	42.8	10.5	1830	−167	48.9	41.5	15	−192	–	–
AADY1	200	0.0	0	0	0.0	0.0	15.6	1673	−318	53.8	38.1	–	–	–	–
	400	0.9	836	323	30.7	57.6	11.1	1732	−229	43.2	35.4	1716	−242	43.0	34.9
	700	0.6	1382	144	29.8	33.7	5.1	3038	−267	43.2	37.7	2695	−278	41.2	35.4
AADY1-re	200	0.3	369	55	28.7	34.1	11.4	2065	−312	56.9	42.0	2050	−348	56.8	40.7
	400	1.2	1118	145	35.7	43.4	9.9	2500	−178	49.3	43.1	2500	−245	49.3	41.3
	700	0.9	1417	329	30.2	41.0	7.8	3240	−195	44.3	40.1	3130	−270	43.7	38.1
AADY2	200	0.3	367	60	28.6	34.6	15.6	1522	−222	52.4	40.0	–	–	–	–
	400	1.2	988	308	33.5	57.5	15.6	1625	−52	42.1	40.0	–	–	–	–
	700	1.5	1313	315	28.9	39.1	15.6	1900	113	35.2	38.2	–	–	–	–
ASSC	200	0.3	776	68.4	41.3	48.3	8.7	1497	−17	52.1	50.8	1490	−21	52.0	50.5
	500[a]	0.9	1765	224	39.7	49.6	15.6	2183	141	43.3	48.8	–	–	–	–
	800[b]	1.2	2149	500	35.0	51.4	6.0	2502	436	37.6	50.8	2425	431	37.0	50.1
ASSC-re	500	0.3	1675	228	38.8	49.0	15.0	3170	46	49.5	51.0	3170	43	49.5	50.9
	800	2.4	1741	529	31.4	49.7	10.5	1835	515	32.3	49.7	1788	515	31.9	49.3
ADBS1	200	0.3	476	66	32.9	39.8	3.0	1904	−277	55.7	41.8	1475	−287	51.9	37.0
	400	0.6	456	175	21.3	30.2	5.1	2320	−225	48.0	40.5	1885	−245	44.6	36.4
	700	0.6	1049	330	25.4	35.9	5.4	2970	−195	42.8	38.6	2594	−220	40.5	35.8
ADBS2	200	0.3	471	70	32.7	40.1	2.7	1910	−270	55.8	42.1	1475	−288	51.9	37.0
	400	0.3	706	150	28.0	35.8	3.6	2230	−190	47.4	40.8	1935	−220	45.0	37.5
	700	0.6	1076	330	25.8	36.3	8.1	2580	−112	40.4	37.9	2520	−120	40.0	37.3
AAA	300	0.3	533	150	28.1	39.8	3.0	1729	−130	47.9	41.9	1560	−162	46.2	38.9
	500	0.6	1154	255	32.4	44.6	3.0	2448	−90	45.2	42.4	2010	−110	41.9	38.5
	700	0.6	1364	315	29.6	39.7	6.3	2890	−130	42.4	39.4	2735	−152	41.4	38.0
AASK	200	1.5	256	120	23.0	38.0	16.2	320	109	26.4	39.6	320	109	26.4	39.6
	500	3.0	366	392	15.5	39.0	16.2	393	392	16.4	40.2	–	–	–	–
	800	3.3	499	637	13.8	37.2	16.2	538	636	14.6	38.4	–	–	–	–
AASK-re	200	2.4	280	121	24.3	39.7	16.5	315	111	26.1	39.7	–	–	–	–
	500	3.3	381	386	16.0	38.7	16.2	405	394	16.8	41.0	–	–	–	–
	800	1.2	671	580	17.2	37.2	16.2	983	492	22.4	37.9	–	–	–	–
	800	2.7	515	635	14.1	37.6	6.9	557	635	15.0	38.9	–	–	–	–
C.SV	100	3.0	63	77	13.9	35.3	15.0	72	77	15.3	37.6	–	–	–	–
	300	1.8	243	288	16.8	65.5	15.0	320	300	20.4	–	–	–	–	–
	600	4.2	890	318	25.2	37.7	15.0	1250	217	30.7	38.3			–	–
C.SC	200	–	–	–	–	–	11.1	161	161	16.7	42.1	–	–	–	–
	500	–	–	–	–	–	11.1	497	430	19.4	51.3	–	–	–	–
	800	–	–	–	–	–	9.6	957	695	22.0	55.1	–	–	–	–
C.K	450[c]	–	–	–	–	–	18.6	381	362	17.3	43.2	–	–	–	–
	600[d]	4.8	448	496	15.8	43.1	19.8	530	431	17.8	37.6	–	–	–	–

re: repeated.

[a] $B_g = 6.3\%$.

[b] $B_g = 4.9\%$.

[c] $kc = 1.5$.

[d] $B_g = 2.5\%$.

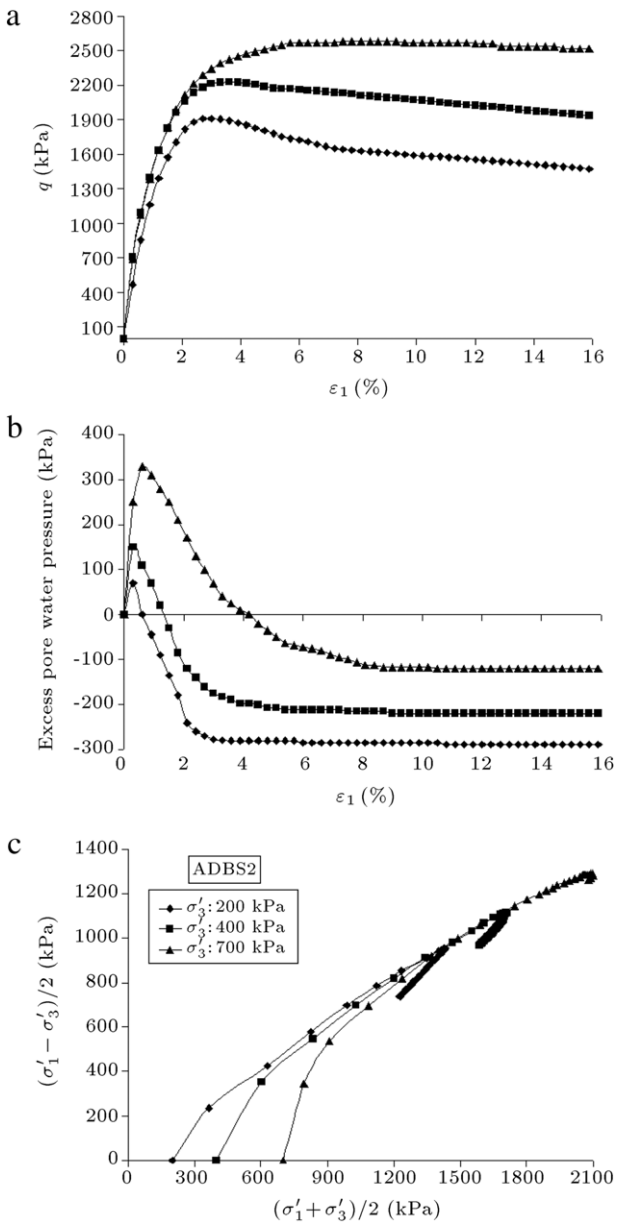

Figure 8: Stress–strain-excess pore water pressure and stress path relationships of ADBS2.

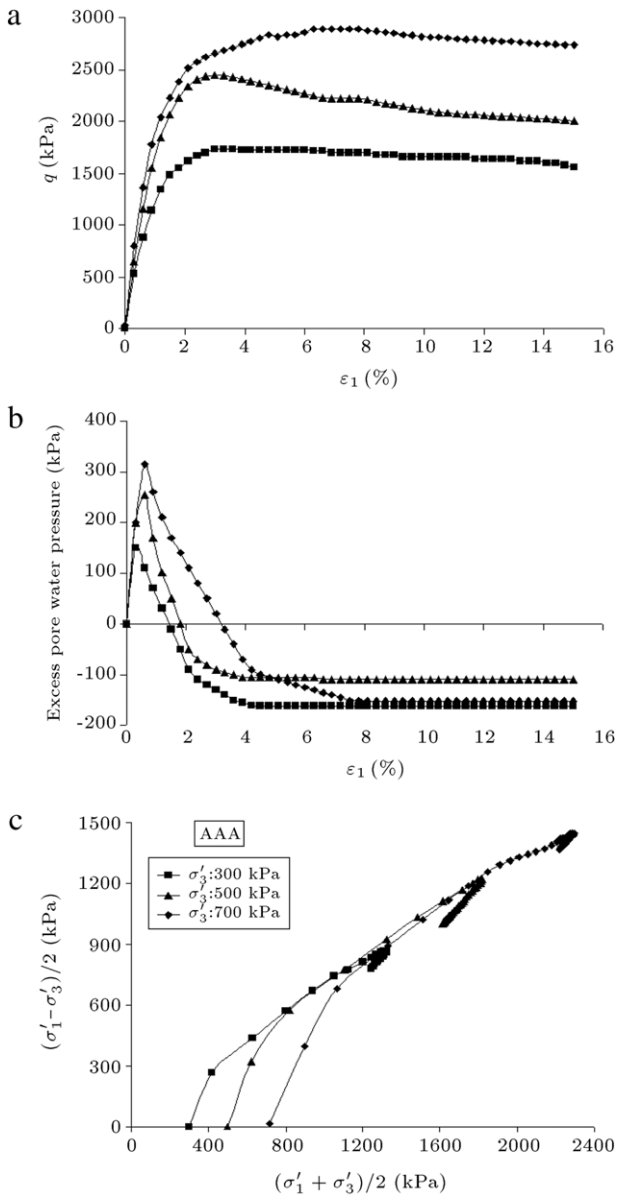

Figure 9: Stress–strain-excess pore water pressure and stress path relationships of AAA.

of material finer than 0.2 mm and having more than 22% of material finer than 0.2 mm. The results indicate that the q/σ_3' values, for the gravelly materials having less than 10% of material finer than 0.2 mm is considerably higher than those of the gravelly materials having more than 22% of material finer than 0.2 mm. The q/σ_3' values at u_{max} and low confining pressure are considerably smaller than the values at q_{max} for the materials having less than 10% of material finer than 0.2 mm. Moreover, q/σ_3' values at $q_{residual}$ for the materials having less than 10% of material finer than 0.2 mm only at low confining pressures are slightly smaller than those of q_{peak}.

ϕ and ϕ' versus σ_3' for each single confining pressure at q_{max} and $q_{residual}$.

The variations of internal friction angle versus confining pressure at total and effective stress conditions for the gravelly materials are presented in Figure 16. Friction angles are calculated for each single confining pressure, assuming $c = 0$, and using the following equations:

$$\sin\phi = \frac{\sigma_1 - \sigma_3}{\sigma_1 + \sigma_3}, \qquad \sin\phi' = \frac{\sigma_1' - \sigma_3'}{\sigma_1' + \sigma_3'}. \tag{1}$$

Figure 16(a) indicates that the internal friction angle at q_{max} and $q_{residual}$ of the gravelly materials having less than 10% of material finer than 0.2 mm decreases with increase in the confining pressure. This is in fact due to the effect of positive excess pore pressure generation. Generally, the total stress internal friction angle (ϕ) for the confining pressures ranging from 100 to 900 kPa for the materials ranges between 58° and 15° and decreases linearly as σ_3' increases. The effective internal friction angle (ϕ') for the confining pressures ranging from 100 to 900 kPa for the materials ranges between 55° and 36°, with

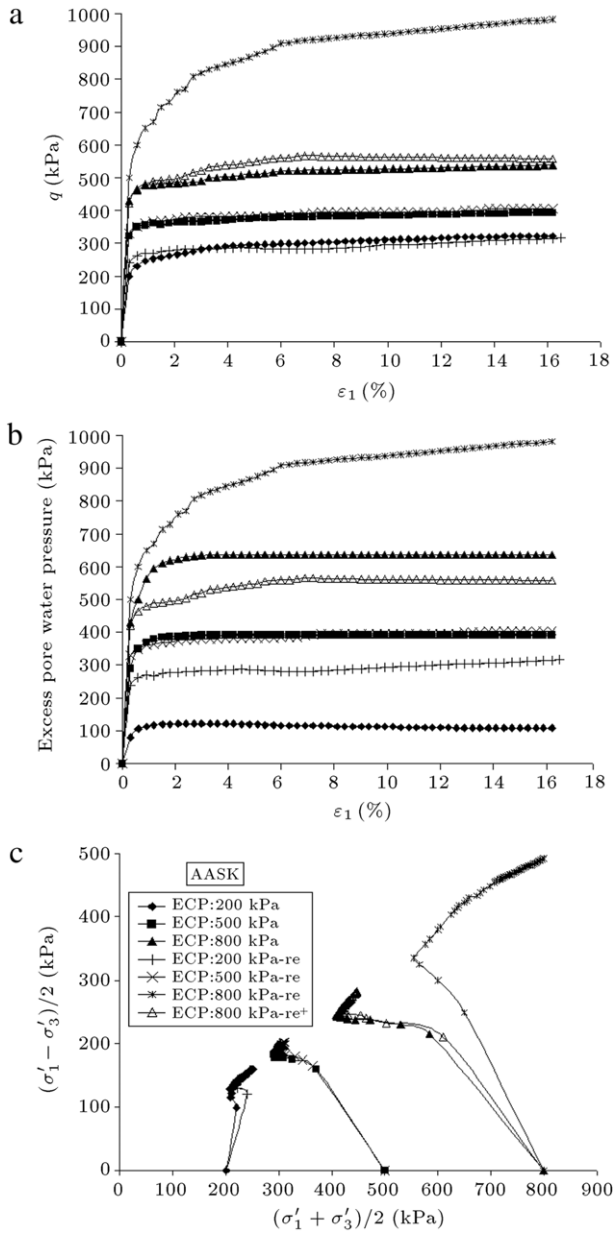

Figure 10: Stress–strain-excess pore water pressure and stress path relationships of AASK.

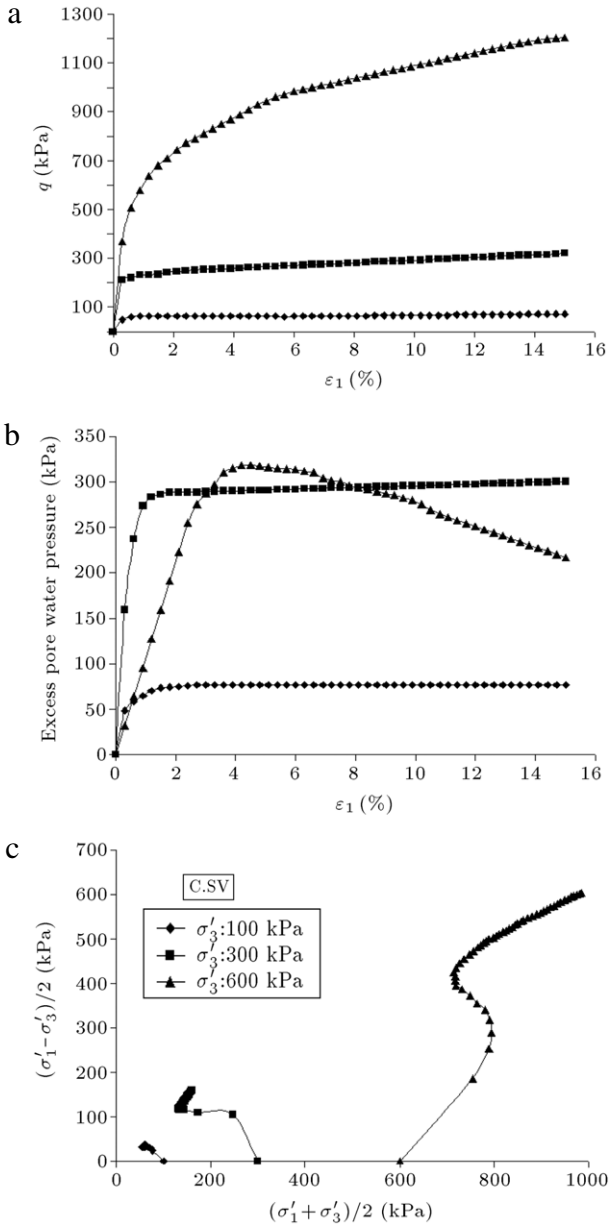

Figure 11: Stress–strain-excess pore water pressure and stress path relationships of C.SV.

an average of 40° in all ranges of the studied confining pressure. Figure 16(b) indicates that the average ϕ at q_{max} and $q_{residual}$ of the gravelly materials having more than 22% of material finer than 0.2 mm is almost constant (about 20°). The average ϕ' value for the gravelly materials having more than 22% of material finer than 0.2 mm is equal to of the materials having less than 10% of material finer than 0.2 mm with an average of 40°. Moreover, the internal friction angle at $q_{residual}$ is slightly lower than that of q_{max}.

Data presented in Tables 1 and 2 suggest that particle gradation has significant effects on the value of the internal friction angle for both *crushed* and *alluvium* materials. Generally, ϕ' for the gravelly materials subjected to a specific confining pressure decreases with increasing size of particle. For example, the internal friction angle decreases by changing from *AADY1* to *AADY2* or from *ADBS1* to *ADBS2* grading (see Figure 1). The above behavior may be attributed to the fact that particle breakage potential in materials with relatively larger particles is comparatively higher.

5.3. Effects of passing 0.2 mm and PI on $q_{residual}/2\sigma'_3$ and $\phi_{q_{peak}}$

The variations of $\phi_{q_{peak}}$ versus the passing 0.2 mm and Plasticity Index (PI) of the soils is shown in Figure 17. Selecting 0.2 mm as a separator diameter was base on the stress paths behaviors. The results indicate that the general trend of $\phi_{q_{peak}}$ has a tendency to decrease with increasing passing 0.2 mm and PI in total stress, almost the equal value (40°) for different passing of 0.2 mm and PI in effective stress condition.

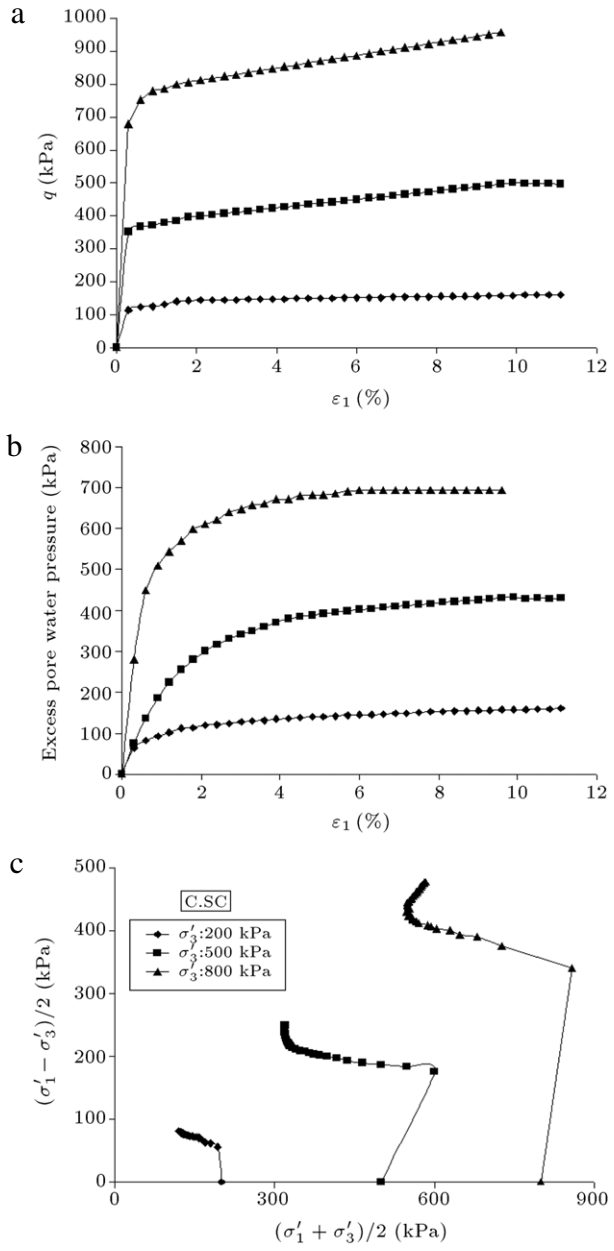

Figure 12: Stress–strain-excess pore water pressure and stress path relationships of C.SC.

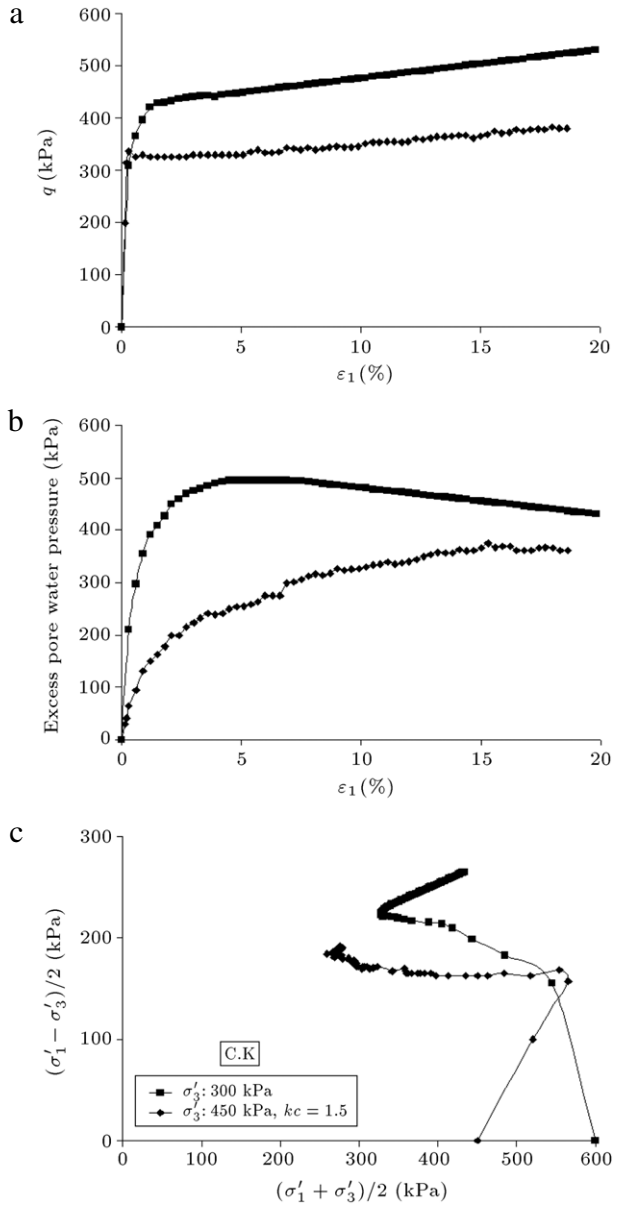

Figure 13: Stress–strain-excess pore water pressure and stress path relationships of C.K.

The relation of $q_{residual}/2\sigma_3'$ (as indication of undrained residual strength or cohesion) versus PI and passing 0.2 mm of the gravelly soils is shown in Figure 18. The results indicate that the $q_{residual}/2\sigma_3'$ has a tendency to decrease with increasing PI of soils and passing 0.2 mm. Similar trend was observed for sandy silt and silty sand (PI = 0, $S_{us}/\sigma_3' = q_{residual}/2\sigma_3' = 0.1$–$0.19$, and PI = 30, $S_{us}/\sigma_3' = 0.03$) [20]. Moreover, for the gravelly material with high PI and having more than 22% of material finer than 0.2 mm, the value of $q_{residual}/2\sigma_3'$ ranges between 0.33 and 1.

Variations of $q_{residual}/2\sigma_3'$ versus σ_3' are shown in Figure 19. The results indicate that for the gravelly materials having more than 22% of material finer than 0.2 mm, the $q_{residual}/2\sigma_3'$ versus σ_3' relationship is linear and less than that of the gravelly materials having less than 10% of material finer than 0.2 mm, which is nonlinear and decreases as σ_3' increases, and finally two groups get the same value (almost 1) at high confining pressures.

5.4. *c and ϕ by curve fitting of Mohr's stress circles at q_{max}*

Table 3 presents the total and effective cohesions and internal friction angles by curve fitting of Mohr's stress circles at q_{max}.

Variation of cohesion (total and effective) versus passing of 0.2 mm for the gravelly materials by curve fitting of Mohr's stress circles at q_{max} are shown in Figure 20. The results indicate that the apparent cohesions at the studied stress level have considerable values, especially for the material having less than 10% of material finer than 0.2 mm. This subject has great

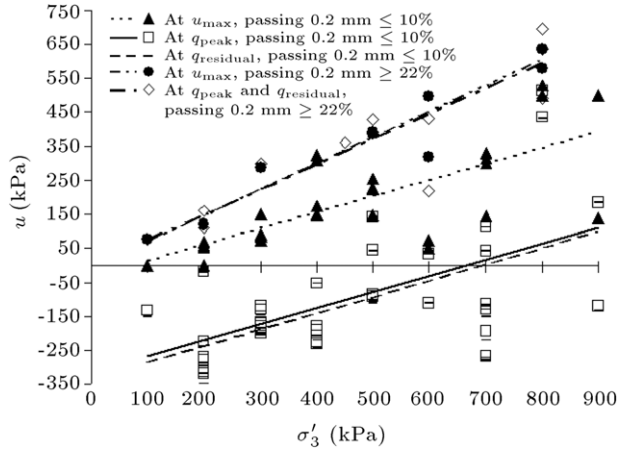

Figure 14: Variations of u versus σ'_3.

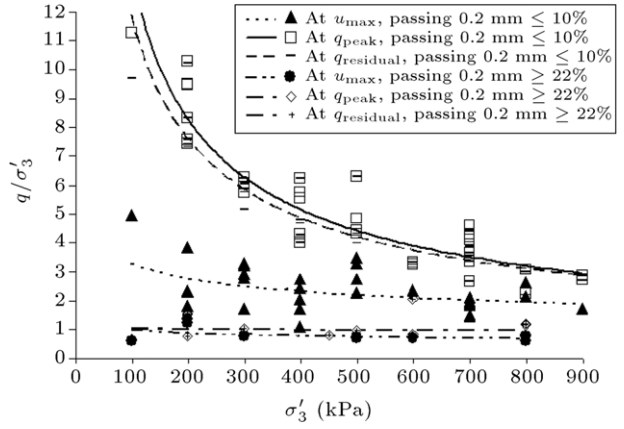

Figure 15: Variations of q/σ'_3 versus σ'_3.

importance in numerical modeling the behavior of gravelly soils at *CU* conditions. Generally, c and c' decrease as passing

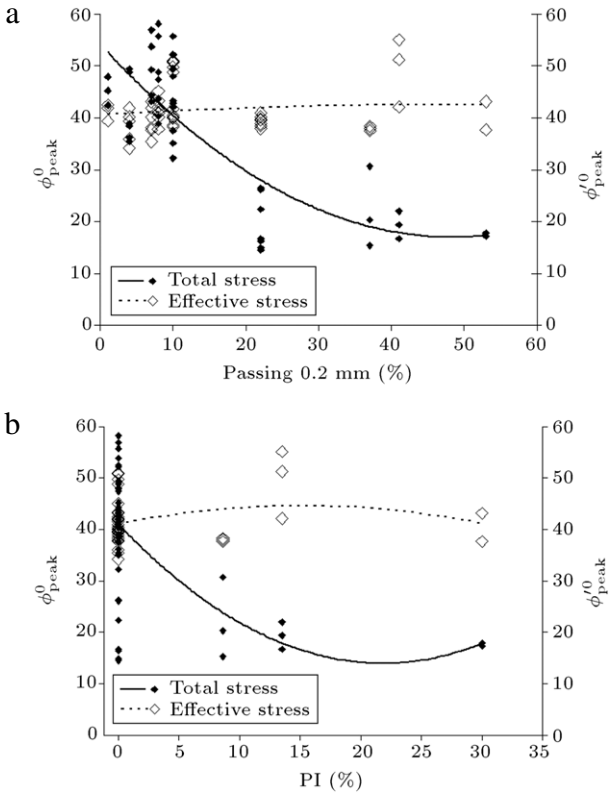

Figure 17: Variations of friction angle based on single point method versus, (a) passing 0.2 mm, and (b) PI.

percentage of 0.2 mm increases, with considerable higher c value at low fine contents.

Figure 21 shows the variations of internal friction angle (total and effective) versus passing of 0.2 mm for the gravelly materials by curve fitting of Mohr's stress circles at q_{max}. The results indicate that ϕ and ϕ' decrease as passing percentage of 0.2 mm increases with considerable higher ϕ and ϕ' values at low fine contents. Generally, the average of ϕ' for the material

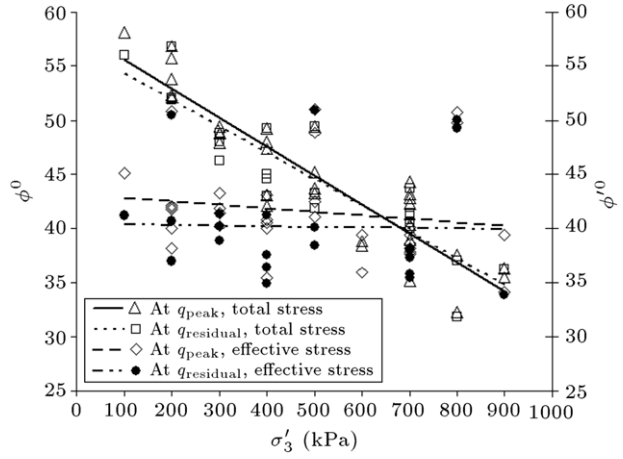

(a) Passing 0.2 mm $\leq$ 10%.

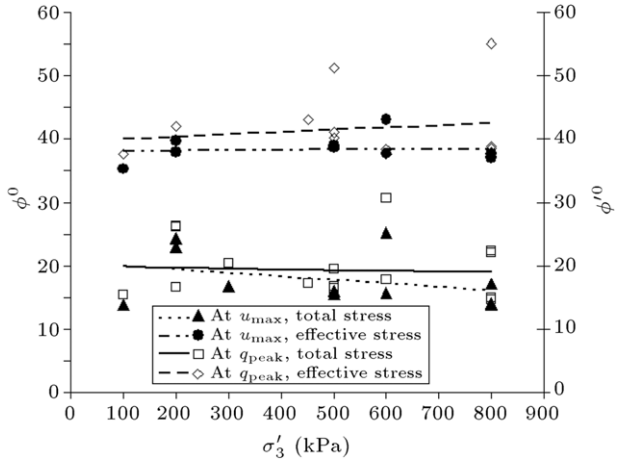

(b) Passing 0.2 mm $\geq$ 22%..

Figure 16: Variations of ϕ and ϕ' versus σ'_3 for the gravelly materials.

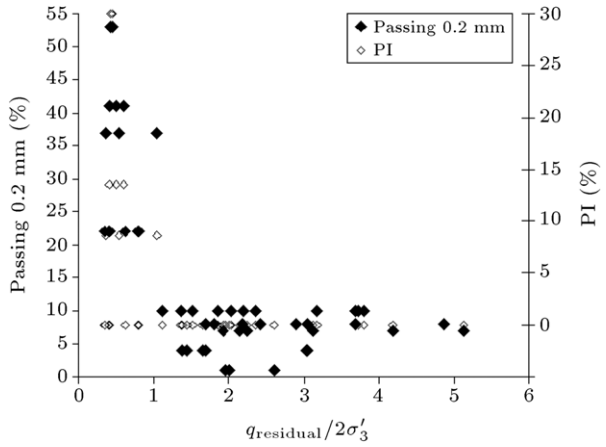

Figure 18: Variations of $q_{residual}/2\sigma'_3$ versus PI and passing 0.2 mm.

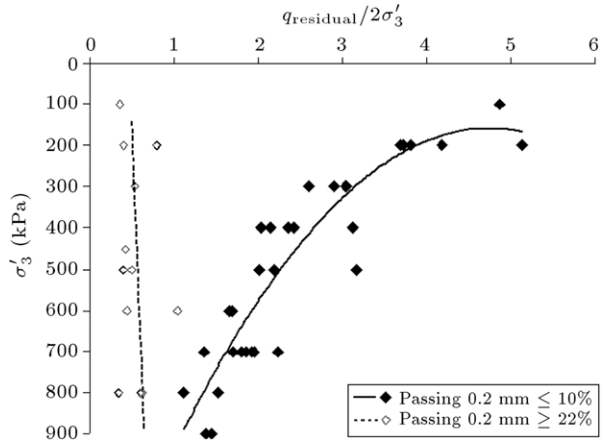

Figure 19: Variations of $q_{residual}/2\sigma'_3$ versus σ'_3.

Table 3: Total and effective cohesions and internal friction angles by curve fitting of Mohr's stress circles at q_{max}.

Gravelly soils	Ranges of σ'_3 (kPa)	ϕ (°)	c (kPa)	ϕ' (°)	c' (kPa)
BABS	300–900	20.7	536.2	36.3	197.5
BABS-re	300–900	25.6	430.4	26.9	358.0
BAA1	100–700	34.5	315.3	42.8	132.3
AADY1	200–700	44.2	218.0	43.8	0.0
AADY1-re	200–700	37.0	453.1	42.4	185.6
AADY2	200–700	16.6	507.1	35.5	174.4
ASSC	200–800	42.6	162.3	57.2	203.0
ADBS1	200–700	34.6	432.7	38.7	200.8
ADBS2	200–700	25.0	551.0	32.3	311.7
AAA	300–700	42.6	244.3	42.5	151.4
AASK	200–800	9.0	100.3	42.5	17.5
AASK-re	200–800	19.5	6.6	43.0	18.7
C.SV	100–600	32.0	0.0	42.3	42.4
C.SC	200–800	22.2	0.0	56.4	90.4
C.K	450–600	18.2	0.0	31.3	66.8

having less than 10% of material finer than 0.2 mm is about 40°, which is equal to the results of each single confining pressure.

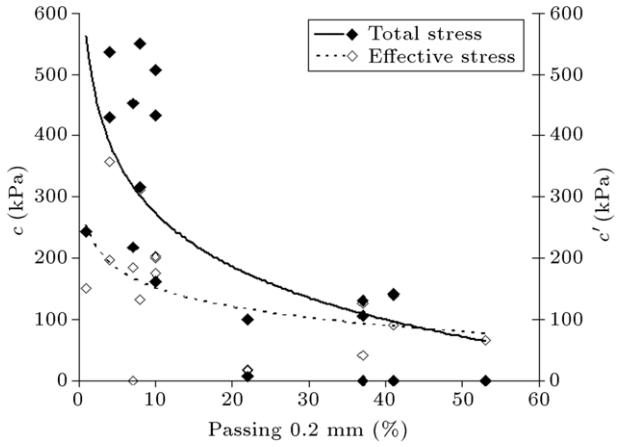

Figure 20: Variations of cohesion (total and effective) versus passing of 0.2 mm for the gravelly materials by curve fitting of Mohr's stress circles at q_{max}.

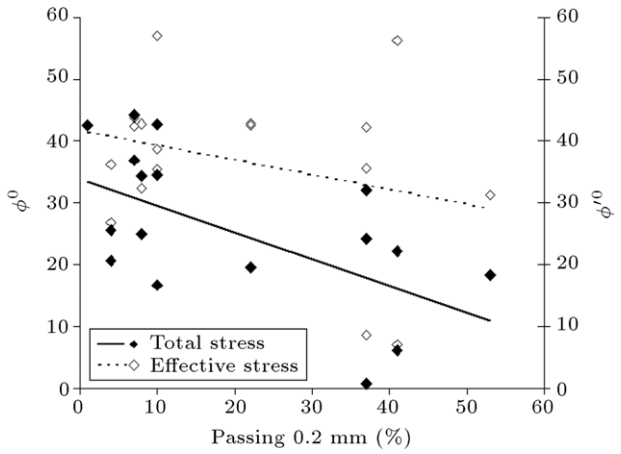

Figure 21: Variation of internal friction angle (total and effective) versus passing of 0.2 mm by curve fitting of Mohr's stress circles at q_{max} for the gravelly materials.

6. Comparison of the CU and CD results

In this study, 26 pairs of the *CD* [9] and *CU* triaxial tests on the same materials were conducted (Table 4). Tests results including deviator stress-volumetric strain-excess pore water pressure and deviator stress ratio (q_{cd}/q_{cu}) versus axial strain are presented in Figures 22–29. Generally, the axial strains at q_{max} in *CD* conditions are lower than those of the *CU* conditions. More interesting, where the volumetric strain in *CD* condition is minimum, the excess pore water pressure in *CU* condition decreases to zero. This phase difference required more attentions. Generally, it is difficult to obtain simple and clear relationship between volumetric strain and excess pore water pressure due to the mentioned phase difference. Moreover, the deviator stress ratio (q_{cd}/q_{cu}) at low axial strain is considerably higher than that of the higher axial strain, which is due to mobilized maximum deviator stress at higher axial strain in *CU* conditions. Generally, at low confining pressure, the deviator stress ratio (q_{cd}/q_{cu}) at low axial is around 1 and less; this means that deviator stress in *CU* conditions is higher than that of the *CD* conditions.

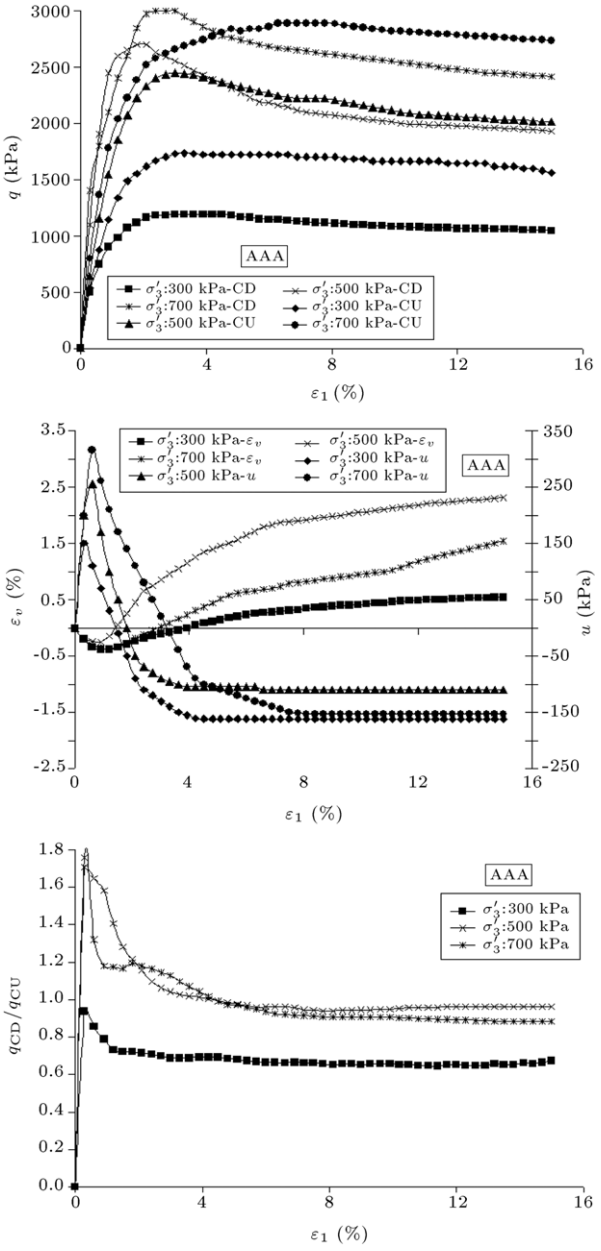

Figure 22: Stress–strain-volumetric strain-excess pore water pressure and deviator stress ratio relationships of AAA at CD and CU conditions.

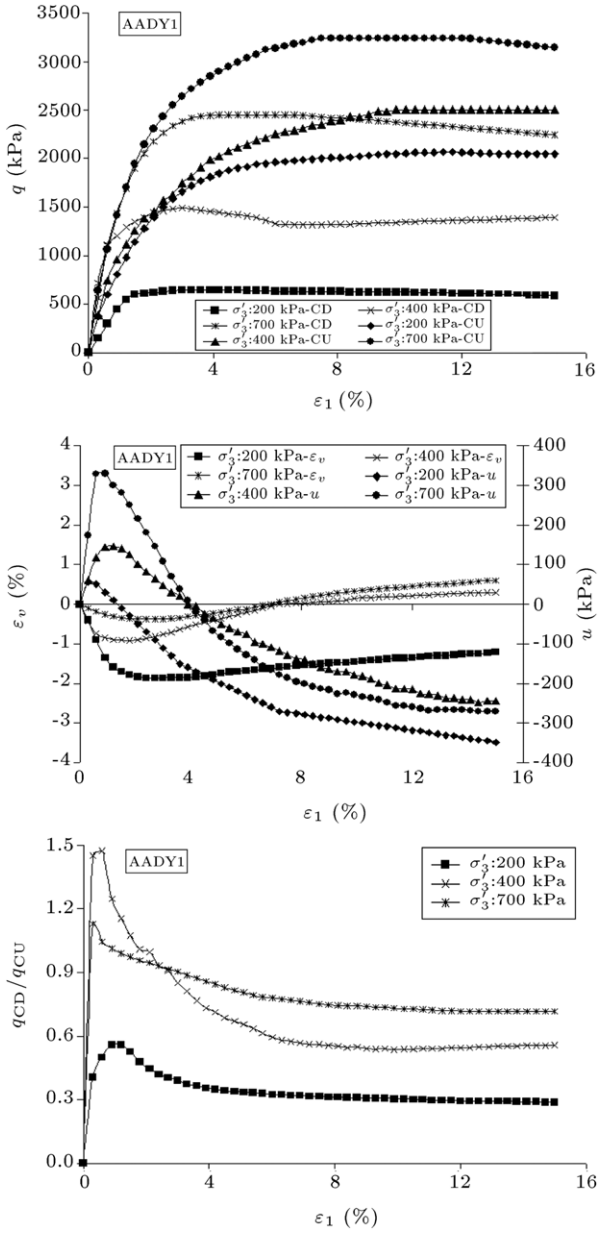

Figure 23: Stress–strain-volumetric strain-excess pore water pressure and deviator stress ratio relationships of AADY1 at CD and CU conditions.

As far as the steady state line is concerned, the two groups' tests results of *CU* and *CD* samples are shown to yield single line (Figure 30).

Figure 31 shows the maximum volumetric strain and maximum excess pore water pressure versus axial strain in *CD* and *CU* conditions. The axial strain related to the maximum volumetric strain in *CD* conditions is considerably higher than that of axial strain at the maximum excess pore water pressure in *CU* conditions. Moreover, there is not a unique relationship between maximum volumetric strain and maximum excess pore water pressure.

Variations of q_{peak} and $q_{residual}$ versus σ_3' in *CD* and *CU* conditions are shown in Figure 32. The deviator stress ratio in CU condition is considerably higher than that of the *CD* condition, especially at low confining pressure. However, as confining pressure increases, the difference become negligible at σ_3' higher than 500 kPa. Moreover, the deviator stress ratio versus σ_3' at $q_{residual}$ is slightly smaller than at q_{peak}.

Figure 33 shows the variation of ϕ' at q_{peak} and $q_{residual}$ versus σ_3' in *CD* and *CU* conditions. The ϕ' value in *CD* conditions is slightly higher than that of the *CU* conditions. Generally, ϕ' decreases as confining pressure increases and ϕ' at $q_{residual}$ is slightly smaller than at q_{peak}.

Variation of ϕ' at q_{peak} versus passing 0.2 mm in *CD* and *CU* conditions is shown in Figure 34. The results indicate that when passing 0.2 mm increases to about 5%, the ϕ' slightly decreases and afterward increases.

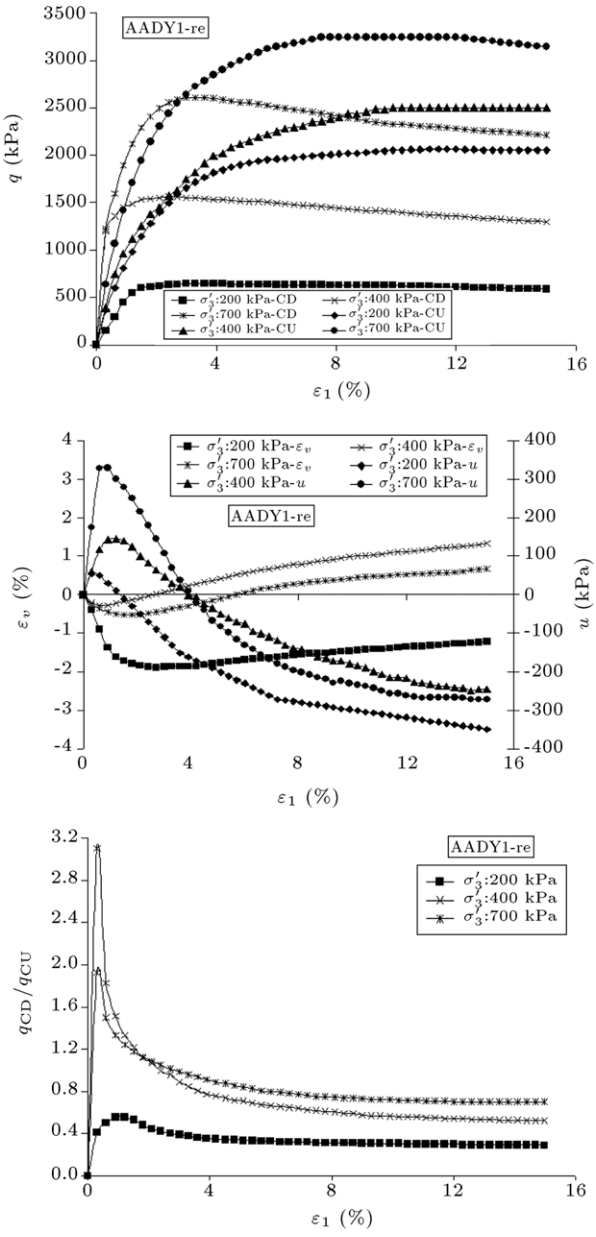

Figure 24: Stress–strain-volumetric strain-excess pore water pressure and deviator stress ratio relationships of AADY1-re at CD and CU conditions.

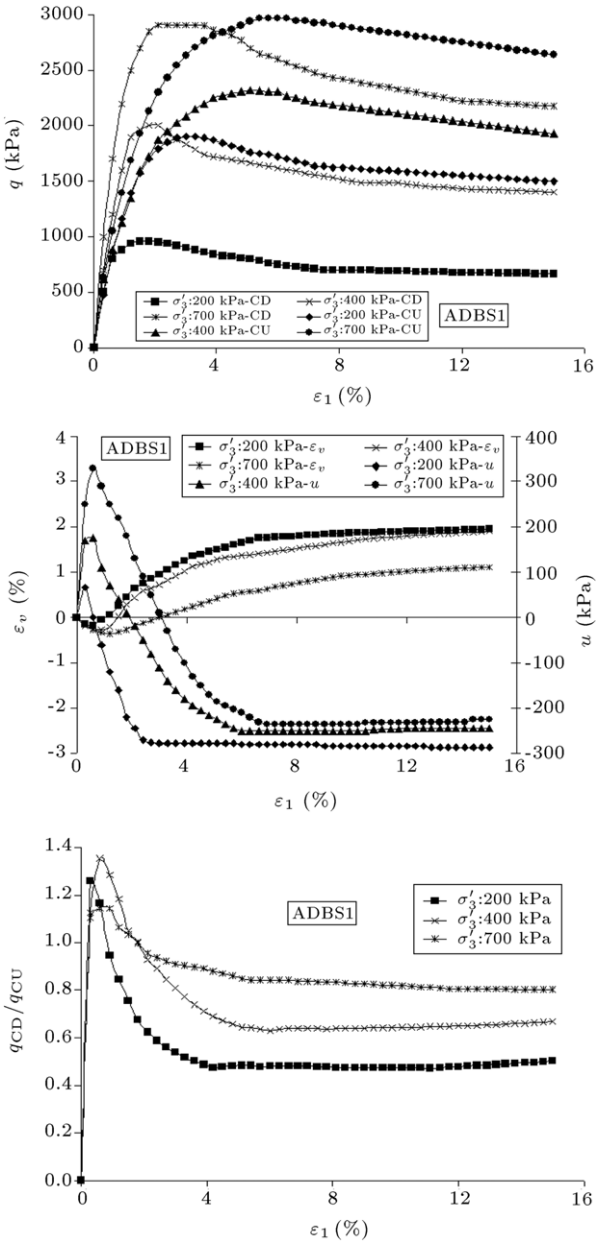

Figure 25: Stress–strain-volumetric strain-excess pore water pressure and deviator stress ratio relationships of ADBS1 at CD and CU conditions.

7. Effect of shape of particle

Figure 35 shows internal friction angle versus confining pressure in *CU* and *CD* conditions for crushed and alluvium materials. The average of ϕ' of *crushed* materials is considerably higher than that of the *alluvium* materials. In general, the reduction rate of ϕ' for the *crushed* materials at low confining pressures is much higher than that of the *alluvium* materials.

8. Effect of point load index and Los Angeles abrasion

Individual particle strength is one of the factors that affects the shear strength of the rockfill materials, in particular as the particle is subjected to high interparticle stresses during shearing. The strength of rock particles is usually evaluated by the Point Load Index test. Figure 36 presents variations of ϕ' versus the ratio of Point Load index to Los Angeles abrasion (I_s/LA) for each of the *crushed* materials. As expected, stiff materials have higher friction angles.

9. Particle breakage

Breakage of the particles was observed during the triaxial tests. The breakage is usually expressed quantitatively by the Breakage Index, B_g [21]. The value of B_g is calculated by sieving the sample using a set of sieves (50–0.075 mm) before and after testing. The percentage of particles retained in each sieve is determined at both stages. Due to breakage of the particles, the percentage of the particles retained in large size of sieves will decrease and the percentage of particles retained in small size sieve will increase. The sum of the decreases will be equal to

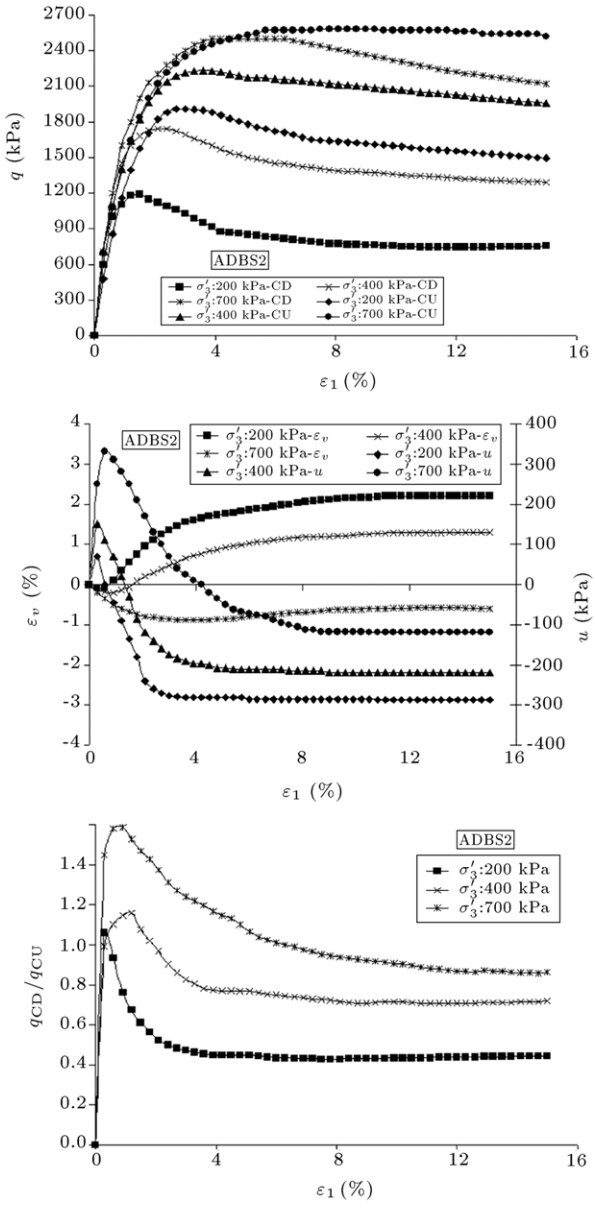

Figure 26: Stress–strain-volumetric strain-excess pore water pressure and deviator stress ratio relationships of ADBS2 at CD and CU conditions.

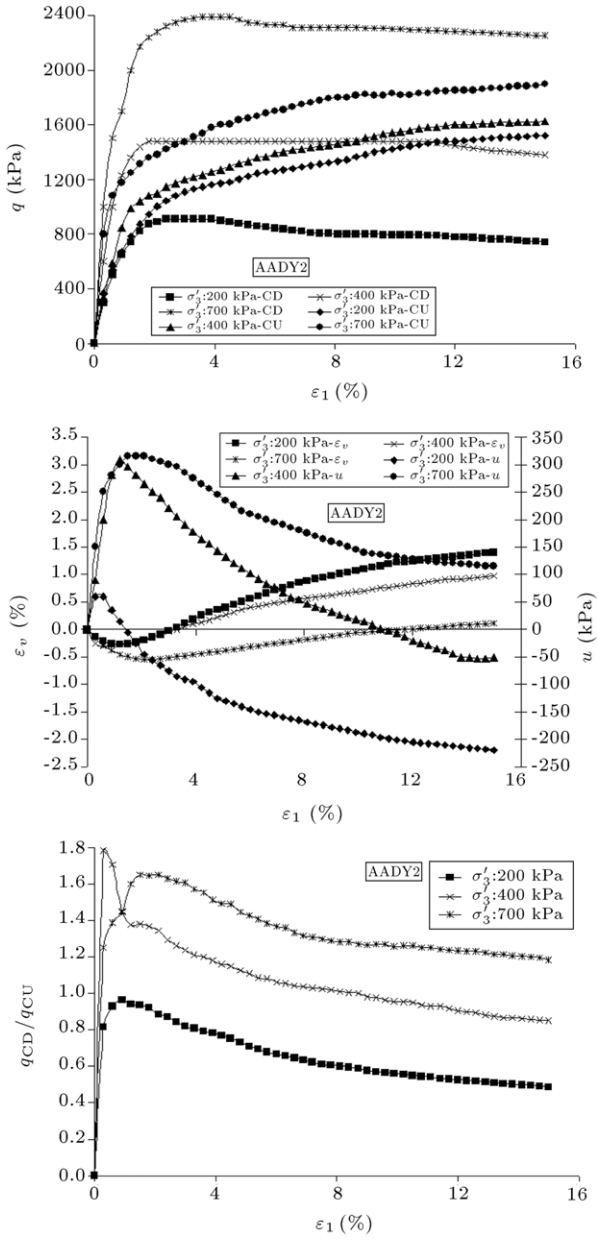

Figure 27: Stress–strain-volumetric strain-excess pore water pressure and deviator stress ratio relationships of AADY2 at CD and CU conditions.

the sum of increases in the percentage retained. The decrease (or increase) is the value of the breakage factor, B_g.

Figure 37 shows variations of the maximum principle stress ratio $(\frac{\sigma'_1}{\sigma'_3})q_{\max}$ versus Marsal Breakage Index (B_g) for the materials. As expected, B_g increases as $(\frac{\sigma'_1}{\sigma'_3})q_{\max}$ decreases. Consequently, it can be inferred that the friction angle decreases with increasing of B_g (see also Table 4).

Figure 38 presents variations of breakage index versus confining pressure for the two test types. Although the data are scattered, B_g increases generally as σ'_3 increases, with a slightly higher rate of increase for the *crushed* materials in *CD* conditions. The effect of particle size and confining pressure on B_g for the *crushed* materials is more significant than for the *alluvium* materials [13,22].

10. Summary and conclusions

This paper presented the results of large scale triaxial testing in undrained conditions on a number of highly compacted gravelly materials specimens with different fine contents, and compared the results with corresponding *CD* conditions. The gravelly materials fall basically into two distinct categories: (1) materials having less than 10% of material finer than 0.2 mm, and (2) materials having more than 22% of material finer than 0.2 mm. The tests results revealed that the strength and deformation parameters of the materials depend on such factors as types and sizes of the particles, confining pressure, Point Load index of the individual particles, and Los Angeles abrasion of the materials. From the tests results the following conclusion may be drawn:

Table 4: Results of triaxial tests on gravelly soils in CD conditions.

Gravelly soils	σ_3' (kPa)	Volume change at end of consolidation (L)	At $\varepsilon_{v(\min)}$				At $q_{\max}$			$\varepsilon_{v\max}$ (%)	At q_{residual}				B_g (%)
			ε_1 (%)	q (kPa)	ϕ' (°)	ε_v (%)	ε_1 (%)	q (kPa)	ϕ' (°)		ε_1 (%)	q (kPa)	ϕ' (°)	ε_v (%)	
BABS	300	0.68	0.6	294	19.2	−0.25	15.0	1009	38.8	1.44	–	–	38.8	–	5.5
	600	1.00	6.9	1860	37.4	−1.58	15.0	2000	38.7	−1.27	–	–	38.7	–	10
	900	0.50	6.3	2650	36.5	−1.72	9.9	2786	37.4	−1.58	15	2783	37.4	−1.27	14
BAA1	100	0.18	0.3	450	43.8	−0.11	2.4	760	52.3	0.95	15	577	48.0	3.53	NIA
	300	0.28	0.9	1200	41.8	−0.19	3.0	1470	45.2	0.22	15	1278	42.9	2.44	4.0
	500	0.39	1.8	2192	43.4	−0.40	4.5	2520	45.7	−0.05	15	2152	43.1	1.96	5.0
	700	0.45	3.0	2952	42.7	−0.86	5.1	3170	43.9	−0.62	15	2704	41.2	0.96	5.0
BAA1-re	300	0.27	1.5	1334	43.6	−0.28	3.3	1523	45.8	−0.11	15	1371	44.1	2.16	NIA
AADY1	200	0.18	–	–	38.0	–	2.7	640	38.0	−1.88	15	598	36.8	−1.22	5.3
	400	0.26	1.8	1393	39.4	−0.91	3.0	1489	40.6	−0.76	15	1394	39.4	0.29	NIA
	700	0.54	2.4	2270	38.2	−0.39	3.9	2445	39.5	−0.32	15	2246	38.0	0.60	6.3
AADY1-re	200	0.16	–	–	38.0	–	2.7	640	38.0	−1.88	15	598	36.8	−1.22	NIA
	400	0.26	0.6	1360	39.0	−0.28	2.4	1560	41.4	−0.03	15	1295	38.2	1.32	NIA
	700	0.54	1.8	2410	39.2	−0.52	3.3	2610	40.6	−0.36	15	2211	37.8	0.67	NIA
AADY2	200	0.15	–	–	44.0	–	2.4	910	44.0	−0.15	15	742	40.5	0.11	NIA
	400	0.24	0.6	1000	33.7	−0.29	2.1	1480	40.5	−0.18	15	1380	39.3	0.97	NIA
	700	0.54	2.4	2320	38.6	−0.54	3.6	2390	39.1	0.12	15	2253	38.1	1.40	7.7
ADBS1	200	0.12	0.6	800	41.8	−0.18	1.5	960	44.9	0.25	15	665	38.6	1.95	NIA
	400	0.20	0.9	1600	41.8	−0.28	1.8	2000	45.6	0.28	15	1402	39.5	1.90	NIA
	700	0.35	1.2	2500	39.9	−0.36	2.1	2910	42.5	−0.19	15	2180	37.5	1.11	NIA
ADBS2	200	0.16	0.6	1000	45.6	−0.09	1.5	1190	48.5	0.55	15	753	40.8	2.20	NIA
	400	0.24	0.9	1450	40.1	−0.20	2.1	1740	43.2	0.20	15	1289	38.1	1.30	NIA
	700	0.27	3.3	2450	39.5	−0.88	3.9	2500	39.9	−0.88	15	2120	37.0	−0.60	3.1
AAA	300	0.60	0.9	900	36.9	−0.38	3.0	1190	41.7	−0.11	15	1148	41.1	0.54	NIA
	500	0.35	0.9	2450	45.2	−0.25	1.8	2700	46.9	0.25	15	1930	41.2	2.30	NIA
	700	0.45	0.9	2100	36.9	−0.38	2.4	3000	43.0	−0.12	15	2415	39.3	1.54	NIA

NIA: no information available.

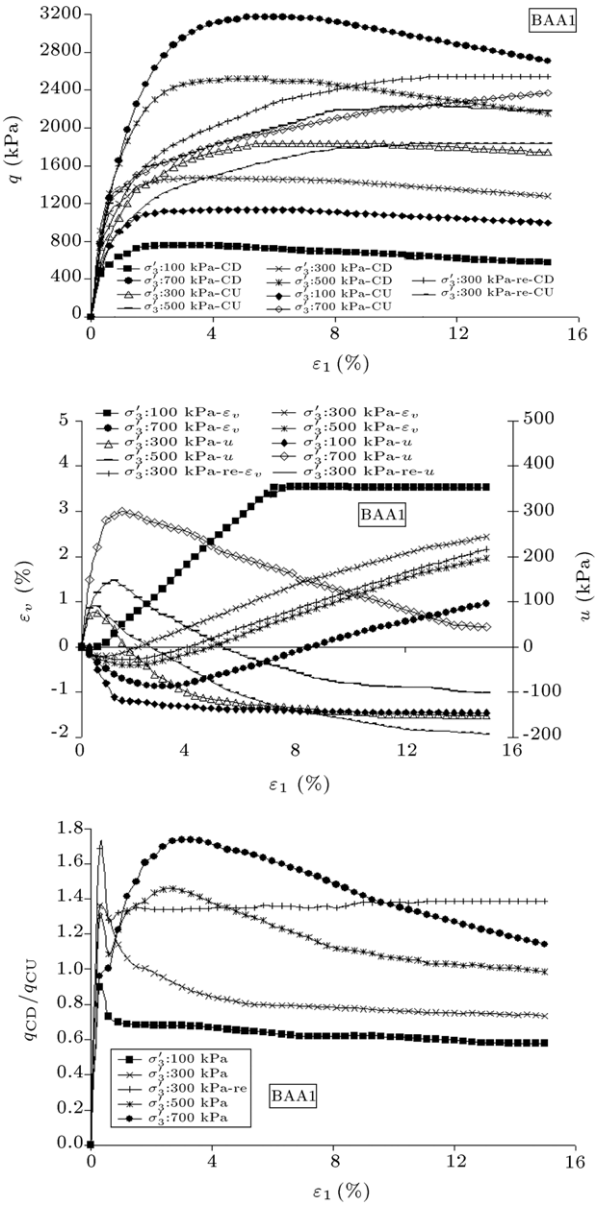

Figure 28: Stress–strain-volumetric strain-excess pore water pressure and deviator stress ratio relationships of BAA1 at CD and CU conditions.

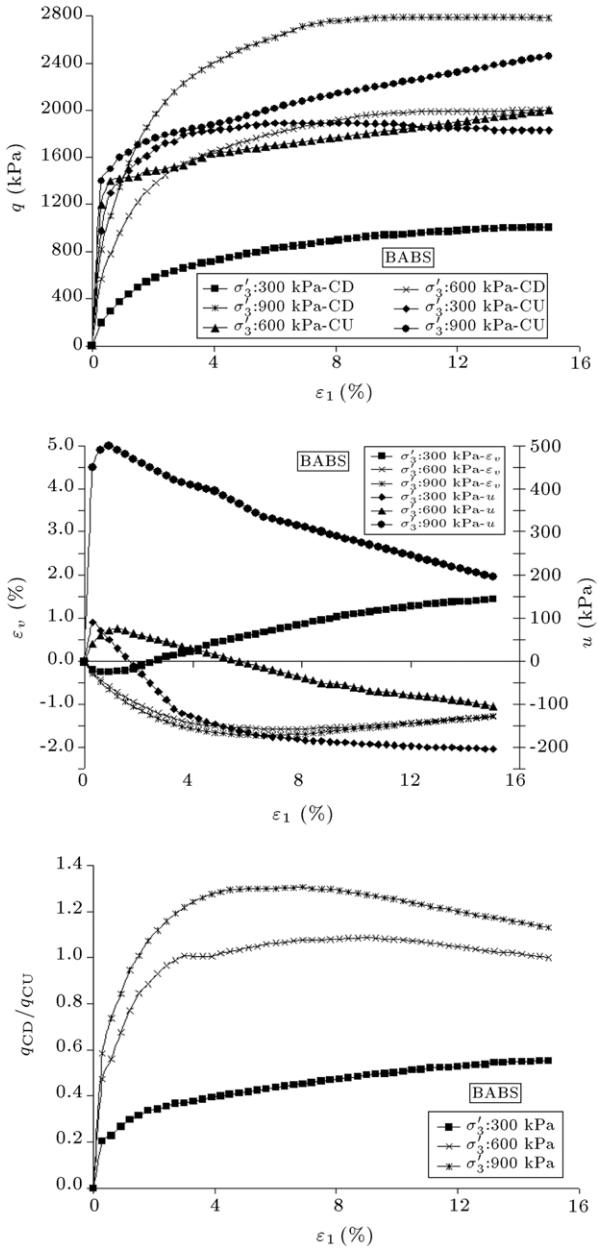

Figure 29: Stress–strain-volumetric strain-excess pore water pressure and deviator stress ratio relationships of BABS at CD and CU conditions.

- The highly compacted gravelly soil specimens have shown dilative behavior at failure state even for materials containing up to 53% passing 0.2 mm.
  Passing 0.2 mm of gravelly soils has considerable effects on the stress path behavior. The $s' - \tau$ stress path of the material having less than 10% of material finer than 0.2 mm has always dilative behavior.
- Maximum excess pore water pressure is positive and increases as σ'_3 increases.

Excess pore water pressure of the gravelly materials having more than 22% of material finer than 0.2 mm at maximum deviator stress and residual deviator stress are identical and positive and higher than u_{max} for the gravelly materials having less than 10% of material finer than 0.2 mm.

- The stiffer materials, as defined by the Point Load Index and Los Angeles abrasion, have relatively higher friction angles.
- $\phi_{q_{peak}}$ decrease with increasing passing 0.2 mm and plasticity index (PI) in total stress.

$q_{residual}/2\sigma'_3$ values decrease with increasing plasticity index of soils and passing 0.2 mm. In the gravelly materials having more than 22% of material finer than 0.2 mm the $q_{residual}/2\sigma'_3$ versus σ'_3 relationship is linear and less than of the gravelly materials having less than 10% of material finer than 0.2 mm, which is nonlinear and decreases as σ'_3 increases, and finally the two groups get the same value (almost 1) at high confining pressures. For the gravelly materials with higher PI and having more than 22% of material finer than 0.2 mm, the value of $q_{residual}/2\sigma'_3$ is ranges between 0.33 and 1.

- The ϕ' value in *CD* conditions is slightly higher than of the CU conditions.

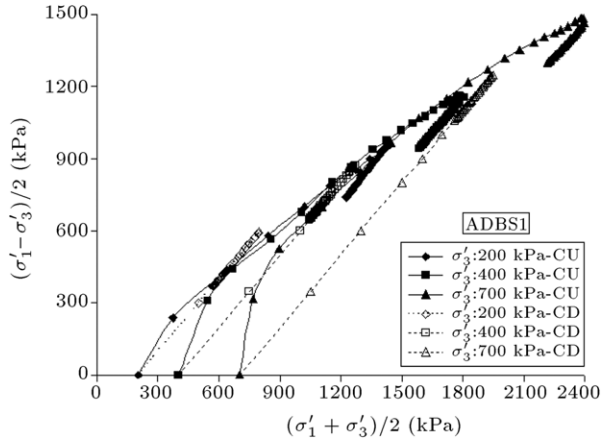

Figure 30: Stress path relationships of ADBS1 in CU and CD conditions.

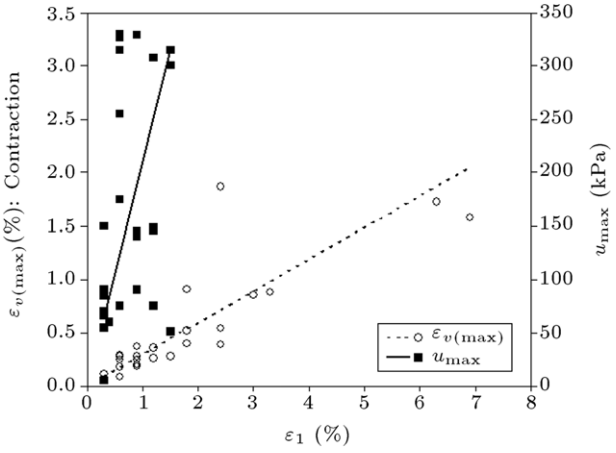

Figure 31: Maximum volumetric strain and maximum excess pore water pressure versus axial strain in CD and CU conditions.

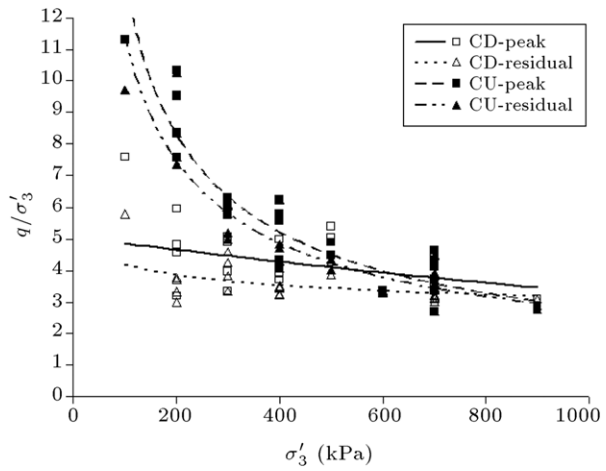

Figure 32: Variation of q_{peak} and $q_{residual}$ versus σ_3' in CD and CU conditions.

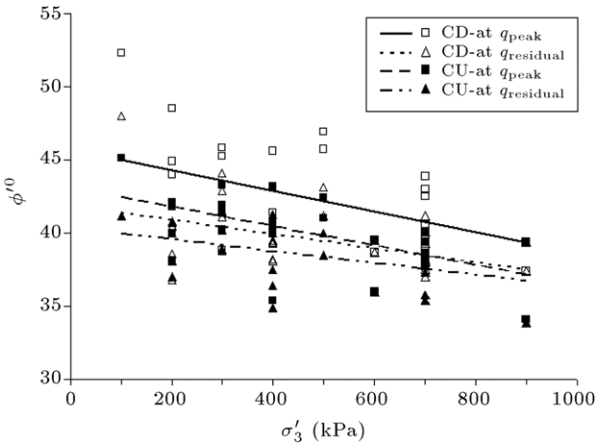

Figure 33: Variation of ϕ' versus σ_3' at q_{peak} and $q_{residual}$ in CD and CU conditions.

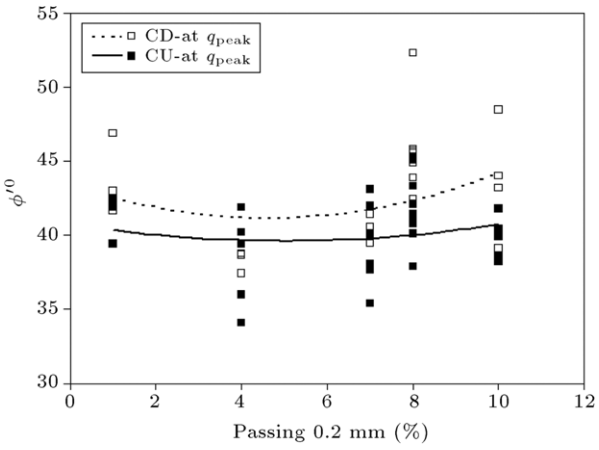

Figure 34: Variation of ϕ' at q_{peak} versus passing 0.2 mm in CD and CU conditions.

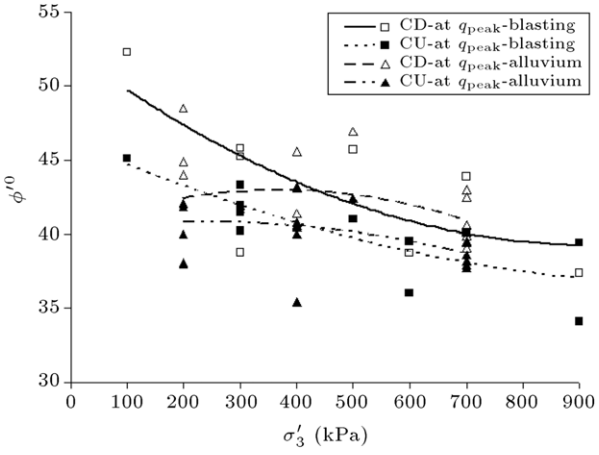

Figure 35: Internal friction angle versus confining pressure in CU and CD conditions for blasting and alluvium materials.

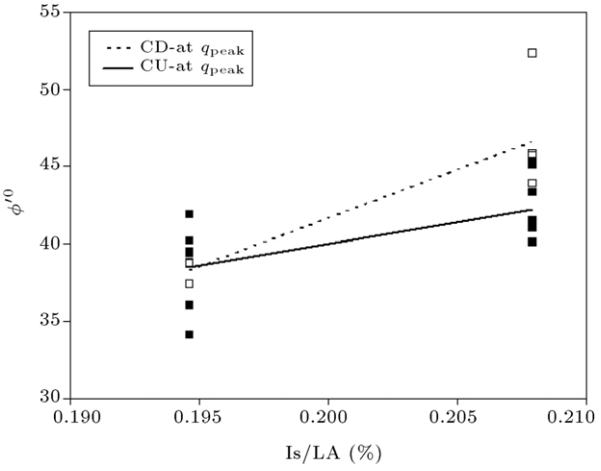

Figure 36: Variation of ϕ' versus I_s/LA for the gravelly materials.

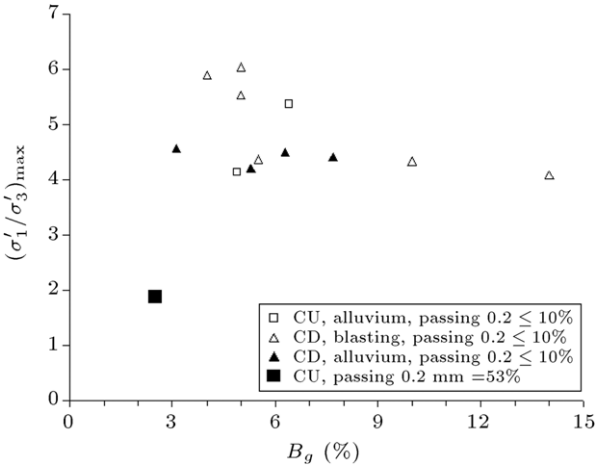

Figure 37: Variations of maximum principle stress ratio $(\sigma'_1/\sigma'_3)_{max}$ versus B_g.

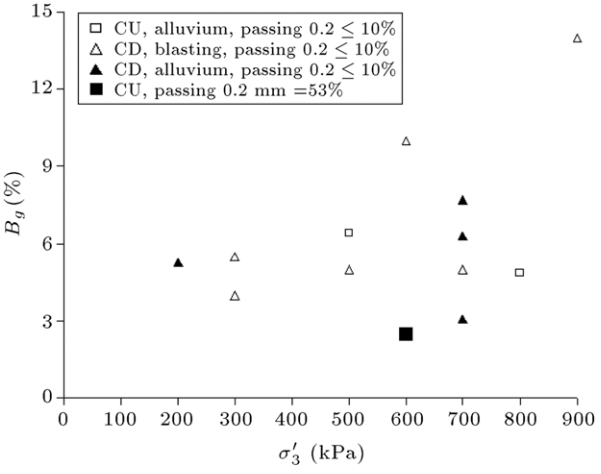

Figure 38: Variations of maximum Breakage Index (B_g) versus σ'_3.

- Generally, the internal friction angle of the *crushed* materials decreases with increasing of confining pressure, whereas the *alluvium* materials show mixed trends in their friction angle behavior, depending on their confining pressures, stiffness and particle breakage.
- Where the volume strain in *CD* conditions is minimum, the excess pore water pressure in *CU* conditions decreases to zero. It is difficult to obtain simple and clear relationship between volumetric strain and excess pore water pressure due to the mentioned phase difference. Moreover, the deviator stress ratio (q_{cd}/q_{cu}) at low axial strain is considerably higher than that of the higher axial strain, which is due to mobilized maximum deviator stress at higher axial strain in *CU* conditions.

Acknowledgments

This research work was supported by *BHRC* under grant 1-1520 (2009). The authors are also thankful to Iran Water Resources and Development Company, as the projects client, for financial aid and providing data for this research. The first author is thankful for the technical help and assistance provided by his respected colleague at the Department of Geotechnical Engineering of *BHRC*.

References

[1] Rashidian, M., Ishihara, K., Kokusho, T., Kanatani, M. and Toshiro, O. "Undrained shearing behavior of very loose gravelly soils", In *Static and Dynamic Properties of Gravelly Soils*, In *Geotechnical Special Publication*, vol. 56, pp. 77–91, (1995).
[2] Zeller, J. and Wullimann, R. "The shear strength of the shell materials for the Ge-Schenenalp Dam", *Proc., 4th Inst., J. SMFE, London*, 2, Switzerland, pp. 399–404 (1957).
[3] Lowe, J. "Shear strength of coarse embankment dam materials", *Proc., 8th Int. Congress on Large Dams*, 3, pp. 745–761 (1964).
[4] Fumagalli, E. "Tests on cohesionless materials for rockfill dams", *J. Soil Mech. Found. Eng., ASCE*, 95(1), pp. 313–332 (1969).
[5] Frost, R.J. "Some testing experiences and characteristics of boulder-gravel fills in earth dam", *ASTM Spec. Tech. Publ.*, 523, p. 207 (1973).
[6] Hirschfield, R.C. and Poulos, S.J. "High pressure triaxial tests on the compacted sand and undisturbed silt. In Laboratory shear testing of soils", *ASTM Spec. Tech. Publ.*, 361, pp. 329–339 (1963).
[7] Bilam, J. "Some aspects of the behavior of granular materials at high pressures". In *Stress-Strain Behavior of Soils: Proceedings of the Roscoe Memorial Symposium, Cambridge*, R.H.G. Parry and G.T. Foulis, Eds., Co. Ltd., Henley-on-Thames, UK, pp. 69–80 (29–31 March 1971).
[8] Lade, P.V., Yamamuro, J.A. and Bopp, P.A. "Significance of particle crushing in granular materials", *J. Soil Mech. Found. Eng., ASCE*, 122(4), pp. 309–316 (1996).
[9] Aghaei-Araei, A., Soroush, A. and Rayhani, M.H.T. "Testing and numerical modeling of rounded and angular rockfill materials", *Sci. Iran.*, 17(3), pp. 169–183 (2010).
[10] Indraratna, B. and Salim, W. "Modeling of particle breakage of coarse aggregates incorporating strength and dilatancy", *Proc. Inst. Civ. Eng.*, 155(4), pp. 243–252. London (2002).
[11] Miura, N. and O-hara, S. "Particle crushing of decomposed granite soil under shear stresses", *Soils Found.*, 19(3), pp. 1–14 (1979).
[12] Russell, A.R. and Khalili, N. "A bounding surface plasticity model for sands exhibiting particle crushing", *Can. Geotech. J.*, 41, pp. 1179–1192 (2004).
[13] Varadarajan, A., Sharma, K.G., Venkatachalam, K. and Gupta, A.K. "Testing and modeling two rockfill materials", *J. Soil Mech. Found. Eng., ASCE*, 129(3), pp. 206–218 (2003).
[14] Marachi, N.D., Chan, C.K. and Seed, H.B. "Evaluation of properties of rockfill materials", *J. SMFE*, 98(1), pp. 95–114 (1972).
[15] Goto, S., Suzuki, Y., Nishio, S. and Oh Oka, H. "Mechanical properties of undisturbed Tone-River gravel obtained by in-situ freezing method", *Soils Found.*, 32(3), pp. 15–25 (1992).
[16] Aghaei Araei, A., Soroush, A., Tabatabaei, S.H. and Ghalandarzadeh, A. "Assessment of monotonic triaxial behavior of gravelly soils", Research Project, No. 1-1520-2009, BHRC, Iran (2010).
[17] ASTM D4767. "Standard test method for consolidated undrained triaxial compression test for cohesive soils" (2004).
[18] ASTM D5311. "Standard test method for load controlled cyclic triaxial strength of soil" (2004).
[19] Alshibli, K.A., Batiste, S.N. and Sture, S. "Strain localization in sand: Plane strain versus triaxial compression", *J. Geotech. Geoenviron. Eng., ASCE*, 129(6), pp. 483–494 (2003).
[20] Ishihara, K.G., *Soil Behavior in Earthquake Engineering*, Clarendon Press, Oxford (1996).
[21] Marsal, R.J. "Large scale testing of rockfill materials", *J. Soil Mech. Found. Eng., ASCE*, 93(2), pp. 27–43 (1967).

[22] Gupta, A.K. "Effect of particle size and confining pressure on breakage and strength parameters of rockfill materials", *Electron. J. Geotech. Eng.*, 14, pp. 1–12. Bund. H (2009).

Ata Aghaei Araei received his Ph.D. from Iran University of Science and Technology (IUST), Iran, in 2011. He was also Ph.D. Researcher at the Geotechnical Laboratory of Civil Engineering at The University of Tokyo. He is a Faculty Member of the Road, Housing and Urban Development Research Center (BHRC) in Iran where he has been working as Senior Geotechnical Engineer and Head of the Geotechnical Laboratory since 2003. Dr. Aghaei Araei's primary research interests include: monotonic and dynamic testing on geomaterials, microzonation, and geotechnical equipment construction.

Abbas Soroush is an Associate Professor in the Department of Civil and Environmental Engineering at the Amirkabir University of Technology (Tehran Polytechnic) since 1997. He received his Ph.D. in Geotechnical Engineering under the supervision of Professor N.R. Morgenstern from the Department of Civil and Environmental Engineering, University of Alberta, Canada. His research interests cover a variety of subjects, including numerical modeling of geomaterials and soil structures, especially earth dams. Dr. Soroush is known as an expert in dam engineering and has attended several numbers of international expert panels for reviewing large dams in the country.

Saeid Hashemi Tabatabaei received his Ph.D. from Roorkee University, India, in 1992. He is a Faculty Member of the Road, Housing and Urban Development Research Center (BHRC) in Iran where he has been Head of the Geotechnical Department since 2002. He has over 18 years experience in the field of geotechnical engineering and geotechnical engineering research. He has been involved in over 33 engineering projects in the fields of landslide hazard and risk assessment, slope stability analysis and mitigation, soil improvement, engineering geological mapping for microzonation of rural areas and site investigation.

Abbas Ghalandarzadeh is Associate Professor in the School of Civil Engineering at the University of Tehran, where he is also currently Head of the Soil Mechanics and Centrifuge Laboratory. He received his Ph.D. in Geotechnical Engineering from the University of Tokyo in 1997. He is a Member of the Technical Committee of TC2 of the International Society of Soil Mechanics and Geotechnical Engineering. His research interests are mainly in the area of Experimental Geotechnics, particularly in model and element testing. Dr. Ghalandarzadeh has undertaken much research in the area of Earthquake Geotechnical Engineering including specifically: the dynamic behavior of rockfill dams with asphalt concrete cores, the seismic behavior of quay walls, reinforced earth and piles, and more recently the anisotropic behavior of saturated sands mixed with clay or silt.